Surface Water - Groundwater Interactions in the Upper Blanco River Watershed: Investigating the Origins of the Pleasant Valley Spring System, Hays County, Texas

Radu Boghici

Hays Trinity Groundwater Conservation District, November 2024

SUMMMARY

In 2019, the Hays Trinity Groundwater Conservation District (HTGCD) Board of Directors adopted Rule 16 creating the Regional Recharge Study Zone (RRSZ) to encompass a specific geographic area overlying the Trinity Aquifer and located wholly within the boundaries of the District. HTGCD staff (henceforth referred to as "*the team*") were directed to "*monitor recharge, discharge, spring flow, water quality, and aquifer levels for the five-year period from January 1, 2020, to December 31, 2025 (the "Study Period")*".

The purpose of this paper is to (1) report on the data collection efforts undertaken by the HTGCD team under the Rule 16 mandate; and (2) use the available data to investigate the source of the flow at the Pleasant Valley Spring (PVS) system, the largest water contributor to the flow of the Blanco River downstream from the Fischer Store Road bridge.

The paper will show that the spring system and the Middle Trinity Aquifer (MTA) are closely interconnected and that continued springflow depends to a large degree on the input of groundwater (baseflow) from the MTA.

BACKGROUND

Rural residents of the RRSZ (Figure 1) and of the adjacent areas in Comal and Blanco counties depend on groundwater from the MTA for their domestic and agricultural water supply. This same aquifer is also supplying water to the Pleasant Valley Spring and several other nearby springs draining into the Blanco riverbed just upstream from the Fischer Store Road near Wimberley, Tex. A large fraction (up to 100 percent during drought) of the Blanco River flow reaching Wimberley originates as springflow from the PVS system. Downstream from Wimberley, the flow of the Blanco River is the sole source of continuous recharge to the Edwards Aquifer in southeastern Hays County (Gary et al., 2019).

As the population of western Hays County increases, the demand for groundwater and surface water for municipal, domestic, irrigation, and recreational uses in the RRSZ and beyond will follow the same trend. Therefore, maintaining an adequate groundwater supply in the MTA within RRSZ is a top concern for the water interests in the RRSZ and downstream.

GEOLOGIC AND STRUCTURAL SETTING

The surface geology within the Blanco River watershed in western Hays County consists of the Lower Glen Rose, Hensel, and Cow Creek, formations which together comprise the MTA (see map in Figure 3). The Upper Glen Rose Limestone outcrops away from the Blanco River along the watershed divides and caps the MTA. The Hammett Shale underlies the Cow Creek Formation and forms the base of MTA. The Hammett Shale is not exposed at the surface in the RRSZ and the adjacent area. A stratigraphic column of these units is shown in Figure 3 at right.

Geologic structure and faulting are important because they can greatly impact the flow of groundwater through the aquifer. Structure mapping cited by Gary et al. (2019) indicates the presence of an uplifted block ('horst') delimited by the Blanco County Fault and the Tom Creek Fault Zone (TCFZ) to the east (Figures 2 and 3). Vertical displacement across the faults of the TCFZ ranges from just a few feet to a few hundred feet (Figure 2).

The outcrop of the Lower Glen Rose Formation within RRSZ is punctuated by many dissolution features like caves and sinkholes also known as "karst" (black stars on Figure 3). Based on the state reports filed for water wells drilled in the RRSZ area, karst can reach hundreds of feet down from the outcrop of Lower Glen Rose Formation and into the underlying Hensel and Cow Creek strata. In these areas, karst serves as recharge features for the MTA.

Faults of the TCFZ can serve as pathways for the movement of groundwater, especially when enhanced by the dissolution of the limestone. The PVS system springs and Jacob's Well Spring emerge where the faults intersect their streambeds.

STUDY AREA DELINEATION

The RRSZ is contained entirely within the Blanco River Watershed, which itself is part of the Guadalupe River Basin. Since the hydrologic conditions inside RRSZ (well levels and the flows of the Blanco River) are likely impacted by the hydrologic conditions upstream/upgradient and away from RRSZ, the team thought it reasonable to include data from several Blanco River subwatersheds in the study area. They are: Wanslow Creek, Boardhouse Creek and Little Blanco subwatersheds (Figure 5) spanning Hays, Comal, and

Blanco counties. The team wanted to include as much of the recharge area (the Lower Glen Rose Formation) inside and around the RRSZ as possible. The study area is bounded by hydrological boundaries, i.e., surface water divides all around.

GROUNDWATER-SURFACE WATER INTERACTIONS ALONG THE BLANCO RIVER

From its headwaters in Kendall County downstream to the City of Blanco, and during average and below average rainfall conditions, the riverbed consists of dry stretches alternating with occasional pools of standing water. There the riverbed cuts through compact layers of limestone that allow only limited infiltration of rainfall. Where rainfall infiltration occurs, shallow perched water table aquifers develop that will transmit the recharged water to the riverbed as springs. The springs feeding the river in the City of Blanco are one such instance. (Smith et al., 2014). Downstream from the City of Blanco, at the Narrows, the riverbed begins to cut through fractured limestone and karst, the Blanco River loses flow to riverbed karst features such as Saunders Swallet, and becomes dry again (Figure 2, top).

Beginning a couple of miles upstream from Fischer Store Road, several springs (Park, Little Park, Miller, Gravel Bar, and Pleasant Valley springs constitute the “PVS system”) supply water to the Blanco River. Potentiometric surface mapping and water quality data point at the MTA as the source of the springflow (see pertaining sections below). The most important of the springs is Pleasant Valley Spring, which upwells from a fracture system crossing the riverbed (Figure 4) three-fourths of a mile upstream from Fischer Store Road, where the USGS maintains a streamflow gauge During normal and low-flow conditions, Pleasant Valley Spring (PVS) provides most, if not all the water reaching Wimberley (Figure 6). PVS is the largest Trinity spring and marks the boundary between a perennially flowing section of the Blanco River downstream and losing and gaining stretches upstream (Hunt et al., 2013). The interaction between the MTA and the flow from the PVS system is shown in Figure 7: the flow of the Blanco River as measured by the USGS at Fischer Store Road correlates very well with the changes in the MTA storage as depicted by the water level readings in the Hays

Trinity Groundwater Conservation District's ESD dedicated monitoring well.

After reaching Wimberley, Tex., the Blanco River then flows for another 13 river miles downstream before losing part of its flow to Johnson Swallet, a karst feature in the Edwards Aquifer recharge zone (Smith et al., 2014). The remaining Blanco River flow eventually reaches its confluence with the San Marcos River under high base flow conditions. When the Blanco is flowing less than 50 cfs, no flow makes it past the Edwards Aquifer Recharge Zone.

THE SOURCE OF THE FLOW FROM THE PVS SYSTEM

To determine the source of the springflow from the PVS system, the team collected and analyzed water level and water chemistry data from study area wells.

Potentiometry

During the summer of 2023, the team collected depth to water readings from privately owned domestic wells within the study area. Sites visited are in subdivisions such as Hill Country Ranches, Burnet Ranch, Mustang Valley Trail, Hunter's Ridge, Ledgerock, Fischer (Comal County), and other nearby areas within and surrounding the study area. Additional water well level data were collected from HTGCD permittees and dedicated monitoring well sites. The team also obtained depth to water readings from neighboring districts such as Barton Springs Edwards Aquifer Conservation District and Blanco-Pedernales Groundwater Conservation District, from Dr. Marcus Gary of the Jackson School of Geosciences, and from the Texas Water Development Board's Groundwater Database. The wells had mostly Middle Trinity completions, however the team also took readings in two wells partially tapping the Lower Trinity and received readings from five shallow wells near the City of Blanco for a total of 59 measurements (Appendix A).

The team converted the depth to water well readings into water level elevations by subtracting the depth to water from the sum of land surface elevation and the elevation of the measuring point for each well. Next, the team plotted the wells on a map of the study area

and posted the calculated water level elevations next to each well. Finally, the team hand-contoured equipotentials (lines of equal hydraulic head) comprising the potentiometric surface map (Figure 8).

The potentiometric surface map shows groundwater flowing from higher head elevations (~1200-1300 feet above mean sea level or AMSL) in the western part of the study area in Blanco County to lower head elevations (~900 feet AMSL) in the eastern part of the study area in Hays County near Wimberley. The overall easterly groundwater flow direction is depicted by the flowline (orange arrow) drawn on the map in Figure 8. There is a data gap in eastern Blanco County within the study area. There, the contours are dashed.

Bending in equipotentials (map contours) when intersecting a streambed typically indicates groundwater surface water interactions. The team noticed such instances around the City of Blanco suggesting that a shallow aquifer feeds water to the river (contours bending upstream). Eastwards, the equipotentials seem undisturbed until past the Blanco-Little Blanco rivers confluence where the contours bend downstream suggesting the Blanco River is losing water to the aquifer. The team also noticed that the spacing of the contours (the flow gradient) doesn't change much from west to east—until the 925- and 900-foot contours, which have a much flatter gradient (wide contour spacing). This typically indicates that large volumes of water are flowing through that section of the study area. This finding was expected because karst and faulting are well documented there (see the black dots showing karst on Figure 3). The springs of the PVS system and, by extension, the flow of the Blanco River downstream from PVS, are manifestations of the karst terrain and of the faulting and fracturing of the MTA and are in close hydraulic interaction with it.

The general groundwater flow directions and significant features of the 2023 potentiometric surface map approximate those mapped in previous studies (Figure 9). The similarity to previous studies indicates a consistency of the flow regimes in the study area across varying hydrologic conditions.

Groundwater Chemistry and Isotopy

To help determine the relationship between springflow from the PVS system and the MTA, the team analyzed water quality and isotope data in 80 wells and springs within the study area. The major ion and isotope data are shown in Appendix B. HTGCD staff collected 12

samples during 2023 and had them analyzed by the Lower Colorado River Authority Environmental Lab Services (LCRA ELS) laboratory in Austin, Texas. The remainder of sixty-six water analyses came from the Texas Water Development Board (TWDB) groundwater database. Five samples came from Lower Trinity wells believed to commingle with Middle Trinity waters. For sites sampled and analyzed repeatedly through time, the team used the most recent lab results—except for the springs of the PVS system where the team used all available data regardless of vintage. All samples have data for major ions such as calcium, magnesium, sulfate, chloride, etc. and trace metals (iron, arsenic, lead, copper, etc.). Twenty-nine of them had analyses on either radiogenic (carbon-14, tritium, and strontium-87/86) or stable isotopes (carbon-13, oxygen-18, deuterium), or both. During the 2023 field sampling work, HTGCD staff have also collected well stabilization parameters such as pH, specific conductance, temperature, and dissolved oxygen. Alkalinity titrations were performed by the LCRA ELS lab. All groundwater sampling by HTGCD staff was conducted in accordance with the TWDB field data collection protocols (Boghici, 2003).

Hydrochemical Facies and Total Dissolved Solids

The team initially separated the data based on proximity to the PVS system into Hays County analyses, Blanco County analyses, and PVS system analyses. One sample was collected from the Blanco River at Fischer store Rd. A Durov plot of the major ion data (Figure 10) shows most of the samples, including those from the springs of the PVS system, plotting tightly together, under a hydrochemical facies that is predominantly calcium-bicarbonate. Some of the Blanco County samples seem to display relatively increasing concentrations of magnesium and sulfate with a corresponding facies change to calcium-sulfate or magnesium-sulfate.

To simplify the plot, the team then combined all well water analyses into one “average” sample the team deem to be representative of the general conditions of the MTA around the PVS system. The team kept the spring data and the river sample separate from the average sample. The team replotted the chemistry data in a new Durov plot, (Figure 11), where the “average” sample is shown as a blue diamond. The near coincidence between the chemical composition of spring waters, the “average” sample, and the river sample is evident.

The team plotted the same hydrochemical facies data on a map (Figure 12) to examine their areal distribution. The dots on the map

representing the well locations are color-coded based on their total dissolved solids (TDS) composition. The labels next to the dots indicate the hydrochemical facies at each site. Wells and springs located near the Blanco River and in the Lower Glen Rose Formation (green shading on the map in Figure 12) tend to be fresher (low TDS concentrations) and exhibit predominantly calcium-bicarbonate facies. Similarly, Comal County samples from sites away from the river but within the faulted, karstified area associated with the PVS system springs also show fresh, calcium-bicarbonate-dominated groundwater. In most other wells away from the river and outside the Lower Glen Rose recharge area, TDS concentrations are higher and the hydrochemical facies change to magnesium- and sulfate-dominated groundwater. The high-TDS sites (red dots) in Hays County represent samples from wells where, based on the drillers' reports) Middle Trinity and Lower Trinity groundwaters are likely to commingle.

Isotopic Analyses

The stable isotopes of water deuterium, and oxygen-18 provide effective means of evaluating the origin, movement, and mixing of natural waters. When used in conjunction with radiogenic isotopes, such as carbon-14 and tritium, they help determine the areal distribution and timing of recharge.

The team plotted deuterium versus oxygen-18 of waters sampled from selected PVS system springs, wells, and the Blanco River at Chimney Valley Rd., and compared them with the stable isotope composition of rainwater (the Global Meteoric Water Line or GMWL) in the study area (Figure 13). The data points plot near GMWL, suggesting a meteoric (rainfall-related) origin for both groundwater and springs data. Geochemical interactions between the aquifer material and the groundwater samples are absent. Some of data points appear to lie on a line originating in the samples clustered around the GMWL and extending towards heavier isotope composition below GMWL shown by river sample. This type of data distribution is characteristic for evaporated waters. Samples experiencing lower evaporation rates lie near GMWL towards its lighter end and tend to preserve the composition of rainwater from which they are derived. The Blanco River sample underwent high evaporation and has become isotopically heavier, because evaporation removes the lighter isotopes preferentially. Closer to the GMWL, the team observe samples from springs plotting along the evaporation line in order of their flowrates (Figure 13).

Dating of groundwater using radiogenic isotopes such as carbon-14 and tritium can give indications as to when the water was taken out of contact with the atmosphere, and when it went underground as recharge. Carbon-14 is used for dating groundwater up to 40,000 years old, while tritium can date groundwaters up to 70 years old (Clark and Fritz, 1997). However, both methods present uncertainties in calculating the age of groundwaters and their residence times underground, which is why the best results are obtained when repeated sampling occurs.

Figure 14 shows a map of the carbon-14 activities (as fraction modern carbon, or fmdn) of wells and springs in the study area. The higher the fmdn value, the higher the activity of carbon-14 in the sample and the higher the proportion of recent recharge from rainfall in the sample. Most samples show Carbon-14 activities exceeding 0.80 fmdn (Figure 14 histogram). Carbon-14 activities are higher than 0.70 fmdn at sites closer to the Blanco River and decline to around 0.20-0.25 fmdn away from the river channel and away from the Lower Glen Rose Fm. outcrop. This data distribution pattern suggests that the outcrop of the Lower Glen Rose Fm. functions indeed as an efficient recharge area where groundwater and recharged water mix in variable proportions.

This interpretation is also supported by the distribution of tritium activities in the samples within the study area (Figure 15). All samples on the map have tritium, indicating the MTA in study area has received pre-modern and modern recharge. (The cutoff value is 0.8 tritium units, or TU, per Clark and Fritz, 1997). Almost all tritium samples from sites near the river area have activities of 0.80 TU or higher, which indicates recharge processes have been taking place post 1950 and, most likely, are happening currently.

Both carbon-14 and tritium data suggest the groundwater in the study area is a mixture of older (aquifer-derived baseflow) and younger (recharged) groundwaters, with the “youngest” mixtures being near the Blanco River. There, aquifer-river water mixing is most active. This thesis is illustrated by the changes in carbon-14 and tritium activities in the samples taken from Pleasant Valley Spring in 2012, 2015, and 2023 (Figure 16). There is good correlation between the carbon-14 activities and the spring discharge measurement: the sample taken during 2015 (high flow reading) shows a water that’s “younger” than the 2012 and 2023 samples, both taken during lower river flows. During dry times, and due to reduced recharge rates, a higher proportion of springflow at PVS comes from aquifer baseflow,

which supplies an “older” water. During wet times, carbon-14 and tritium are added to the PVS spring as rainfall recharge, thus resulting in a “younger” mixture.

CONCEPTUAL MODEL FOR THE AQUIFER, SPRING, AND RIVER SYSTEM WITHIN THE STUDY AREA

The potentiometric, geochemical, and isotopic data presented here show an MTA that interacts significantly with the Blanco River particularly in the RRSZ within HTGCD and in Comal County. Geology, karst, faulting, and recharge are important controls on these interactions.

The aquifer recharges by rainfall on the LGR outcrop through karst, and possibly diffuse infiltration elsewhere. Depending on the surface geology, the existence of karst, faulting, and rainfall amounts, the aquifer and Blanco River exchange water along the riverbed where gaining river sections alternate with losing stretches. Groundwater flows due east through the study area and, when intercepted by faulting, fractures and karst, it can discharge at the surface as springs such as those of the PVS system. As illustrated by the geochemical composition of PVS system and the MTA groundwater, there seem to exist two components to the groundwater flow system. One is a regional flow component that supplies the RRSZ with Middle Trinity groundwater from farther away, outside the study area; it can be regarded as “baseflow”, a rather constant, slower-moving supply of groundwater that is older and/or has longer residence times. The second component is local, faster moving and actively recharged. This flow system exists within the LGR outcrop and near the Blanco River. Where in contact, the two flow components can mix. This model is not unlike the one described by Toth (1962) in his work on the theory of regional groundwater flow (Figure 17).

ESTIMATING BASEFLOW CONTRIBUTIONS TO THE FLOW OF BLANCO RIVER

In the previous sections of this paper, the team showed that the MTA and the Blanco River are in close hydraulic communication within most of the study area. As such, having an estimate of the contribution from the aquifer to the total water balance appears to be important from a groundwater management perspective. The team used two methods to try and quantify the surface water-groundwater interactions along the Blanco River upstream of Fischer Store Rd.:

using (1) baseflow separation techniques and (2) geochemical modeling with NETPATH (Plummer et al., 1994). It is important to note that the baseflow values calculated with baseflow separation methods are not fully comparable with the baseflow calculated by geochemical modeling. The former method separates runoff from the aquifer contribution, and counts in the recharge fraction calculated by the latter method.

Baseflow Separation

Baseflow is defined as the portion of the river streamflow that is sourced from an aquifer that is in hydraulic communication with the river. The other portion of the river flow is runoff, the portion of rainwater falling on the watershed that does not infiltrate underground and is being flushed downstream. The purpose of baseflow separation is to tease apart the two components.

To estimate baseflow contributions to flow of the Blanco River as measured at the USGS Fischer Store station, the team tested eleven hydrograph (baseflow) separation methods incorporated in SepHydro, a web-based tool (Danielescu et al., 2018). During no- or low-rainfall periods, the flow of the Blanco River at that gauge is supplied almost entirely by flow from the PVS system of springs.

Of the eleven baseflow separation methods used by SepHydro, the team picked two (Lyne and Hollick, and Pettyjohn and Henning) as the best approximations of the streamflow and aquifer interactions within RRSZ (Figure 18). Baseflow is shown as a red line, while total streamflow is shown as the black line. The gap between the baseflow line and the streamflow represents runoff. The team chose the two methods because they performed well during low streamflow conditions: baseflow equals streamflow, zero runoff. Their estimates for baseflow as a fraction of total flow (also known as baseflow index, or BFI) during high river flows are different, though. The Lyne and Hollick (1979) method computed BFI values as high as 100 percent during river flows greater than 500 ft^3/s. The Pettyjohn and Henning (1979) method yielded BFI values of up to 34 percent for measured river flows exceeding 500 ft^3/s.

Even though the two baseflow separation methods assume diffuse aquifer flow, both could provide useful insights into the hydrology around RRSZ owing to the dual porosity of the MTA. Where rainfall infiltrates through karst features in the MTA outcrops, one can expect a higher proportion of the precipitation to quickly recharge the aquifer and become baseflow as prescribed by Lyne and Hollick.

If precipitation falls on areas not dotted by karst such as Upper Glen Rose outcrops away from the Blanco River Valley, then a smaller fraction of the precipitation reaches the aquifer—up to 34 percent of precipitation according to the model by Pettyjohn and Henning.

Geochemical Modeling

To further test the hypotheses regarding the origin and evolution of groundwater and springflow in the MTA, the team employed the geochemical mass-balance modeling program NETPATH (Plummer et al, 1994) to simulate chemical mixing between the MTA regional (baseflow) component with rainfall. The goal of this modeling exercise was to simulate mixed water compositions that were observed at PVS during 2015 (wet year) and 2023 (dry year) and determine the proportions of each component (endmember) in the mixture. The endmembers used in the simulations were (1) the "average MTA sample" mentioned in the "Hydrochemical Facies" section; (2) an analysis of rainwater in Sonora, Tex., chosen from the USGS National Atmospheric Deposition Program/National Trends Network (NADP) and, (3) PVS water quality data from 2015 and 2023.

To narrow down the mixing model results, one must specify chemical phases and constraints (chemical processes) based on the geochemistry and the saturation indices of the endmembers. Through our analysis of the endmembers, the team determined that the dissolution and/or precipitation of calcite, dolomite, and gypsum adequately describes the chemical processes responsible for the compositions of the endmembers. Figure 19 (left) shows the relationship between the concentration of calcium plus magnesium versus the concentration of bicarbonate in the samples examined in this study. If all calcium and magnesium were derived from calcite and dolomite dissolution, then data would plot along a line with slope 1:1. Many of the samples meet this requirement, however other plot above the 1:1 line, which indicates additional source of calcium and/or magnesium. A potential source of calcium would be from the gypsum derived either from evaporites within the Upper Glen Rose Formation or by MTA groundwaters mixing with upwelling water from the also evaporitic Lower Trinity Aquifer.

To account for the calcium derived from evaporite dissolution, the sulfate concentration is subtracted from the sum of calcium and magnesium, which concentration is then plotted as a function of bicarbonate (Figure 19, right). Most of the water samples plot on or around the 1:1 line, indicating that carbonate and gypsum

dissolution explain much of the variations in calcium, magnesium, sulfate, and bicarbonate- concentrations

Thus, the team used carbonate dissolution and gypsum dissolution as constraints in the geochemical simulation. The team chose calcium, magnesium, and sulfur to be input phases in the models.

The team first ran the “wet year” model by mixing the “average sample” discussed above with the NADP rainwater sample and attempted to replicate the PVS spring water composition from 2015—a wet year. Two models were found to satisfy the constraints (see Figure 20). The team chose model 2 because of a better match between modeled and saturation indices in the final mixture. Model 2 results indicate that PVS as analyzed in 2015 can be explained by a mixing 63 percent “average sample”, (i.e., presumed baseflow from the aquifer) and 34 percent NADP rainwater (i.e., presumed recharge). The team then ran a “dry year” model mixing the “average sample” discussed above with the NADP rainwater sample and attempted to replicate the PVS spring water composition from 2023—a dry year. Again, two models were found to satisfy the constraints (see Figure 21). The team chose model 2 because of a better match between modeled and saturation indices in the final mixture. Model 2 results indicate that the PVS chemistry, as analyzed in 2023 can be explained by a mixing 58 percent “average sample”, (i.e., presumed baseflow from the aquifer) and 41 percent NADP rainwater (i.e., presumed recharge).

It is important to note that the baseflow values calculated with baseflow separation methods are not fully comparable with the baseflow calculated by geochemical modeling. The former method separates runoff from the aquifer contribution and counts in the recharge fraction. The latter method separates the aquifer fraction from recharge.

CONCLUSIONS

The Middle Trinity Aquifer and the Blanco River are in close hydraulic connection throughout most of the study area and form a dynamic system. The aquifer in the study area recharges mainly through the outcrop of the Lower Glen Rose Formation where karst development is most prevalent. Groundwater flows from Blanco County in the west to Hays County in the east. Owing to increased permeability and faulting of the rocks comprising the aquifer, the springs of the Pleasant Valley system discharge in and near the

streambed and supply most of the river flow downstream, especially during drought. The spring water and well water are predominantly fresh, calcium-bicarbonate facies, and actively recharged (young) particularly at the sites closer to the river channel. Based on geochemical models, the groundwater exchange between the Blanco River and the regional MTA groundwater flow could be between the 30 to 50 percent range, depending on flow regimes, with the rest being derived from precipitation recharge. Baseflow separation methods yield baseflow values of up to 100 percent at low river flows and from 1 to 39 percent during high river flows.

ACKNOWLEDGEMENTS

This work would not have been possible without the support of the HTGCD Board of Directors and of the District staff. The team also acknowledges the help of Dr. Marcus Gary, and Messrs. Doug Wierman and Jeff Watson who lent their professional experience and advice during the data interpretation and writeup; of all the property owners who allowed access to their wells for sampling and measuring; and of the Texas Water Development Board, who funded part of the water quality and isotopic analyses.

FUTURE WORK

The team recommends the continuation of data collection within RRSZ, in both the MTA and the Lower Trinity Aquifer, as the Lower Trinity drilling expands. The data should be periodically revisited to supplement the current conceptual model and develop a better one. A study of the MTA recharge rates would be beneficial, as well as conducting aquifer and pump tests to determine aquifer hydraulic properties such as storativity, transmissivity, and hydraulic conductivity. Considering the faulting and dominance of karst geology in the study area, dye tracing tests would be suggested. A longer-term goal would be the recalibration of the BSEACD Trinity groundwater flow model with any new data.

REFERENCES

Boghici, R., 2003, A Field manual For Groundwater Sampling, Texas Water Development Board publication UM-51, 47 p., https://www.twdb.texas.gov/groundwater/docs/ums/um-51.pdf.

Clark, I.D., Fritz, P., 1997, Environmental Isotopes in Hydrogeology, Lewis Publishers, 342 p.

Danielescu, S., MacQuarrie, K.T.B., Popa, A., 2018, SEPHYDRO: A Customizable Online Tool for Hydrograph Separation. Groundwater 56: 589-593. DOI: https://doi.org/10.1111/gwat.12792.

Davidson, S.C., 2008, Hydrogeological characterization of baseflow to Jacob's Well spring, Hays County, Texas. Master's Thesis, Jackson School of Geosciences, University of Texas at Austin. 125 p., https://haysgroundwater.com/wp-content/uploads/2021/09/Davidson-08_thesis_Cypress_Crk_Jacobs_Well.pdf.

Gary, M.O., Hunt, B.B., Smith, B.A., Watson, J.A., and Wierman, D.A., 2019, Evaluation for the Development of a Jacob's Well Groundwater Management Zone Hays County, Texas. Technical Report prepared for the Hays Trinity Groundwater Conservation District, Hays County, Texas. Meadows Center for Water and the Environment, Texas State University at San Marcos, TX. Report: 2019-05. July 2019. 58 p., https://haysgroundwater.com/wp-content/uploads/2021/09/JW-Mgmt-Zone-Report_7.30.19.pdf.

Heath, S.A., Webster, P.J., Gary, Robin H., 2022, July 2021 Potentiometric Surfaces of the Lower and Middle Trinity Aquifers in Southwestern Hays County, Texas, 31 p., https://haysgroundwater.com/wp-content/uploads/2022/01/HTGCDJuly2021_Trinity_potentiometric_surfaces_20220106final.pdf.

Hunt, B.A., Norris, C., Gary, M.O., Wierman, D.A., Broun, A.S., Smith, B.A., 2013, Pleasant Valley Spring: A Newly Documented Karst Spring of the Texas Hill Country Trinity Aquifer, Abstract, GSA South Central Section 47th Annual Meeting https://bseacd.org/uploads/Hunt_etal_2013.pdf.

Lyne V., Hollick M., 1979, Stochastic time-variable rainfall-runoff modelling. Institute of Engineers Australia National Conference. Publ. 79/10, p. 89-93.

Pettyjohn W.A., Henning R., 1979, Preliminary estimate of ground-water recharge rates, related streamflow and water quality in Ohio: Ohio State University Water Resources Center Project Completion Report Number 552, 323 p.

Plummer, L.N., Prestemon, E.C., Packhurst, D.L., 1994, An Interactive Code (NETPATH), for Modeling Net Geochemical Reactions Along a Flow Path, U.S. Geological Survey Water-Resources Investigations Report 94-4169, 130 p.

Smith, B.A. Hunt, B.B, Andrews, A.G., Watson, J.A., Gary, M.O., Wierman, D.A., and Broun, S.A., 2014, Hydrologic Influences of the Blanco River on the Trinity and Edwards Aquifers, Central Texas, USA, *in* B. Andreo et al. (eds.), Hydrogeological and Environmental Investigations in Karst Systems, Environmental Earth Sciences 1 , https://bseacd.org/uploads/Smith et al. 2014 Blanco River Trinity and Edwards Aquifers.pdf, 9 p.

Tóth, J., 1962, A theory of groundwater motion in small drainage basins in central Alberta, Canada, Journal of Geophysical Research, Volume 67, Issue 11, p. 4375-88.

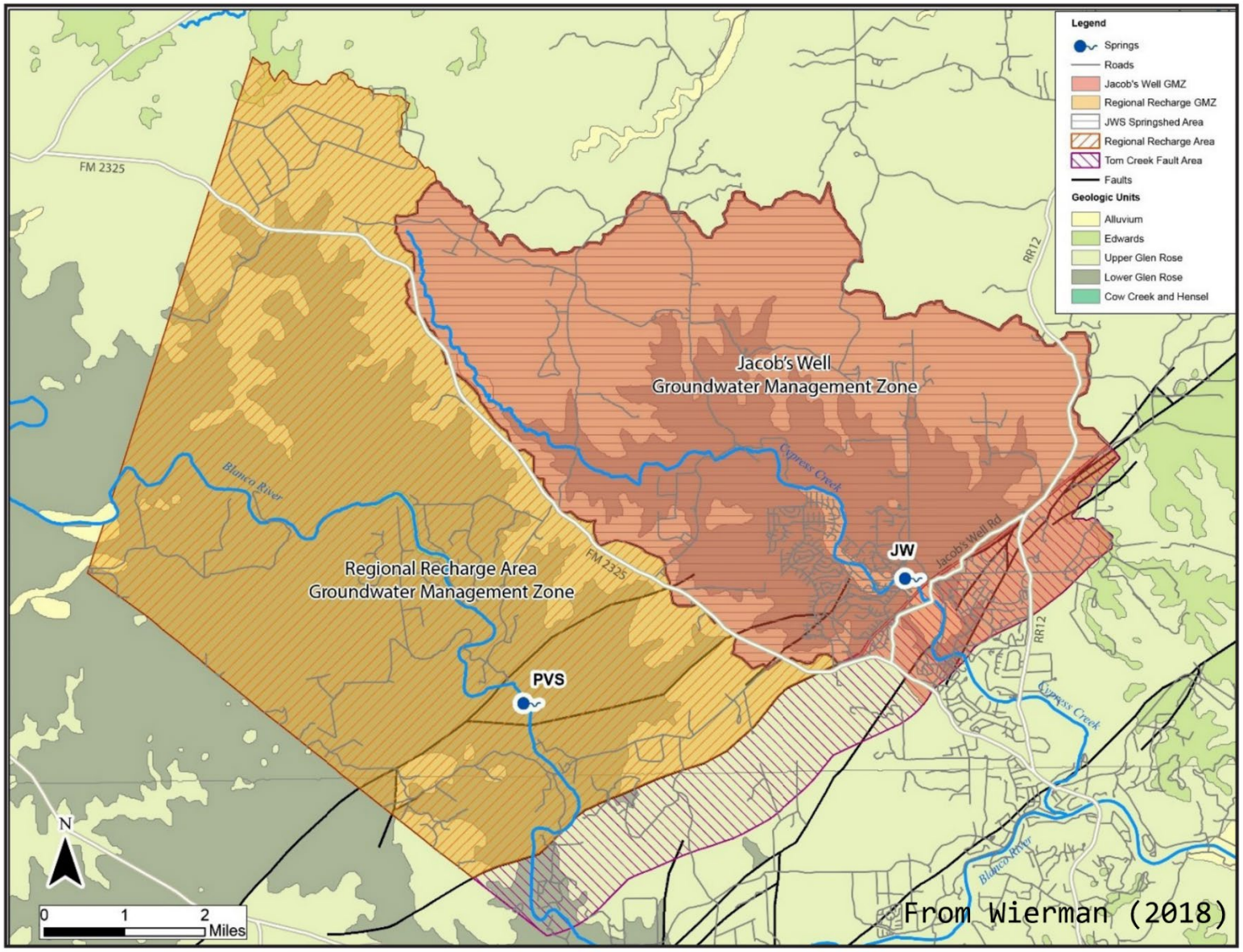

Figure 1. Groundwater management and study zones within Hays Trinity Groundwater Conservation District.

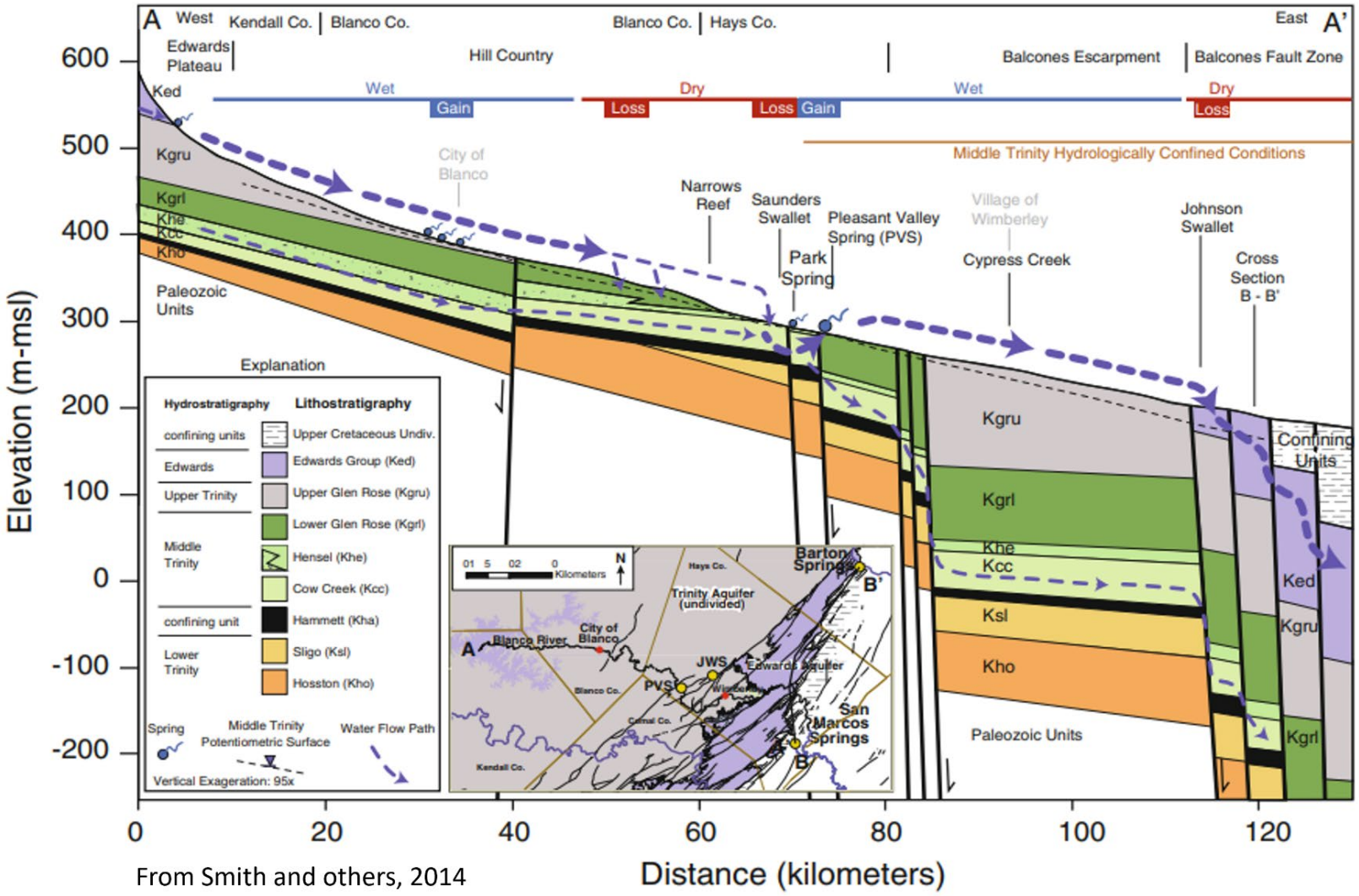

From Smith and others, 2014

Figure 2. Geology, structure, and groundwater-surface water interactions in the Upper Blanco River Watershed.

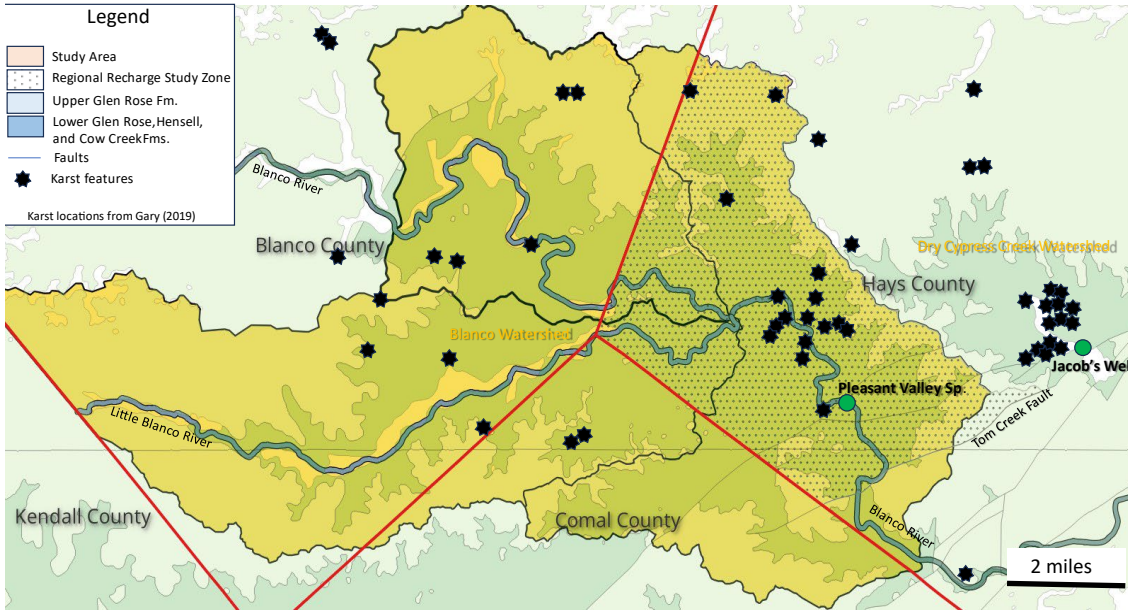

Figure 3. Generalized surface geology, faulting, and karst locations map (above) and stratigraphic column (left).

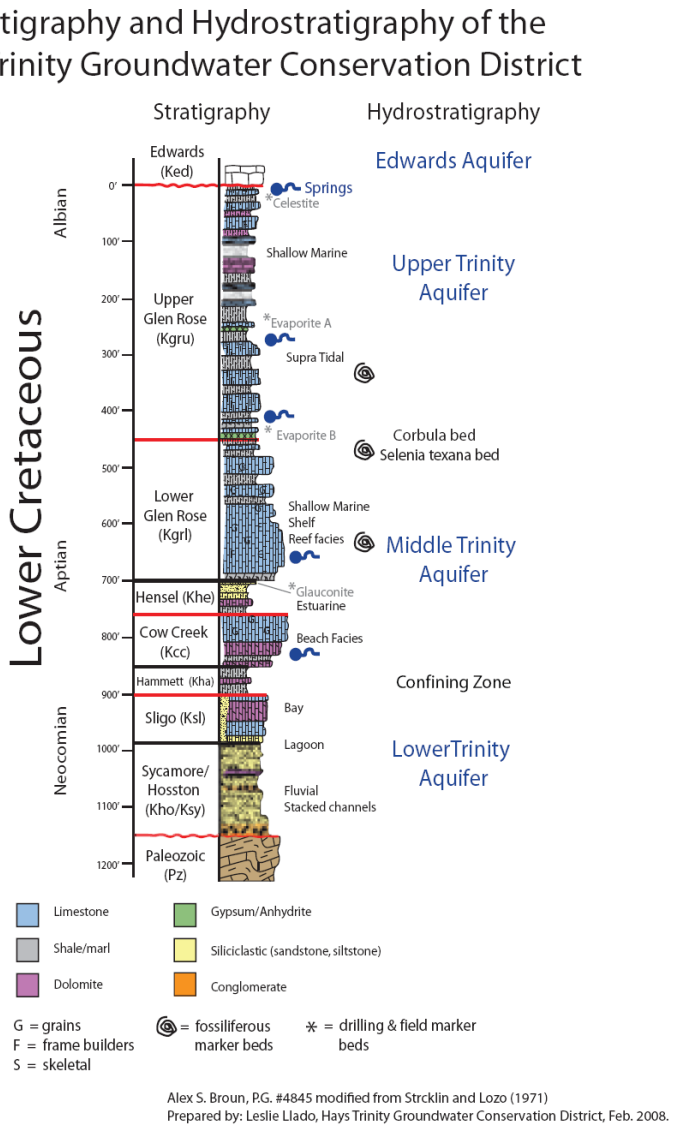

Figure 4. Photographs of the Pleasant Valley Spring emerging in the Blanco River bed. Source: B.A. Smith and others, (2014).

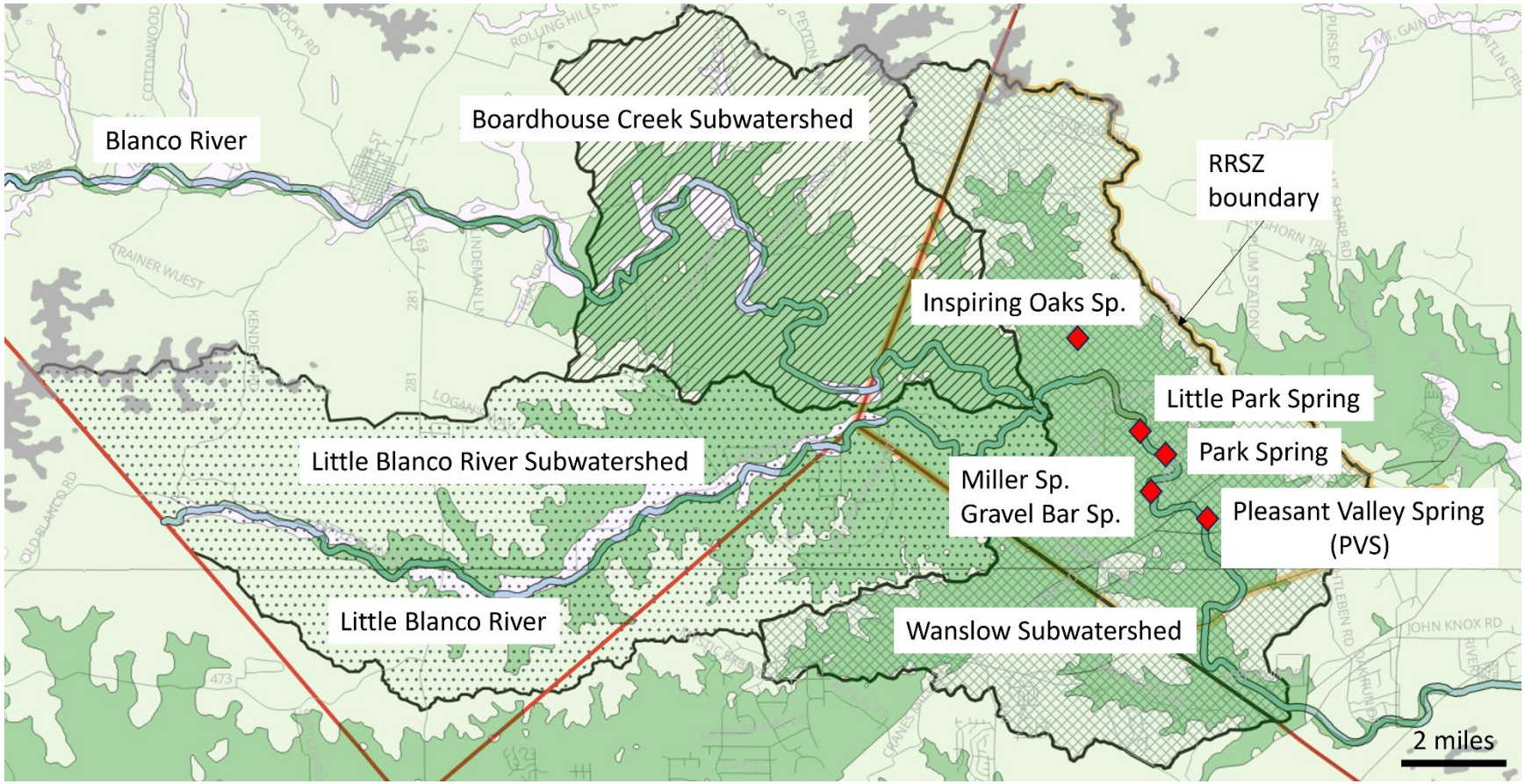

Figure 5. Subwatersheds of the Blanco River included in this study.

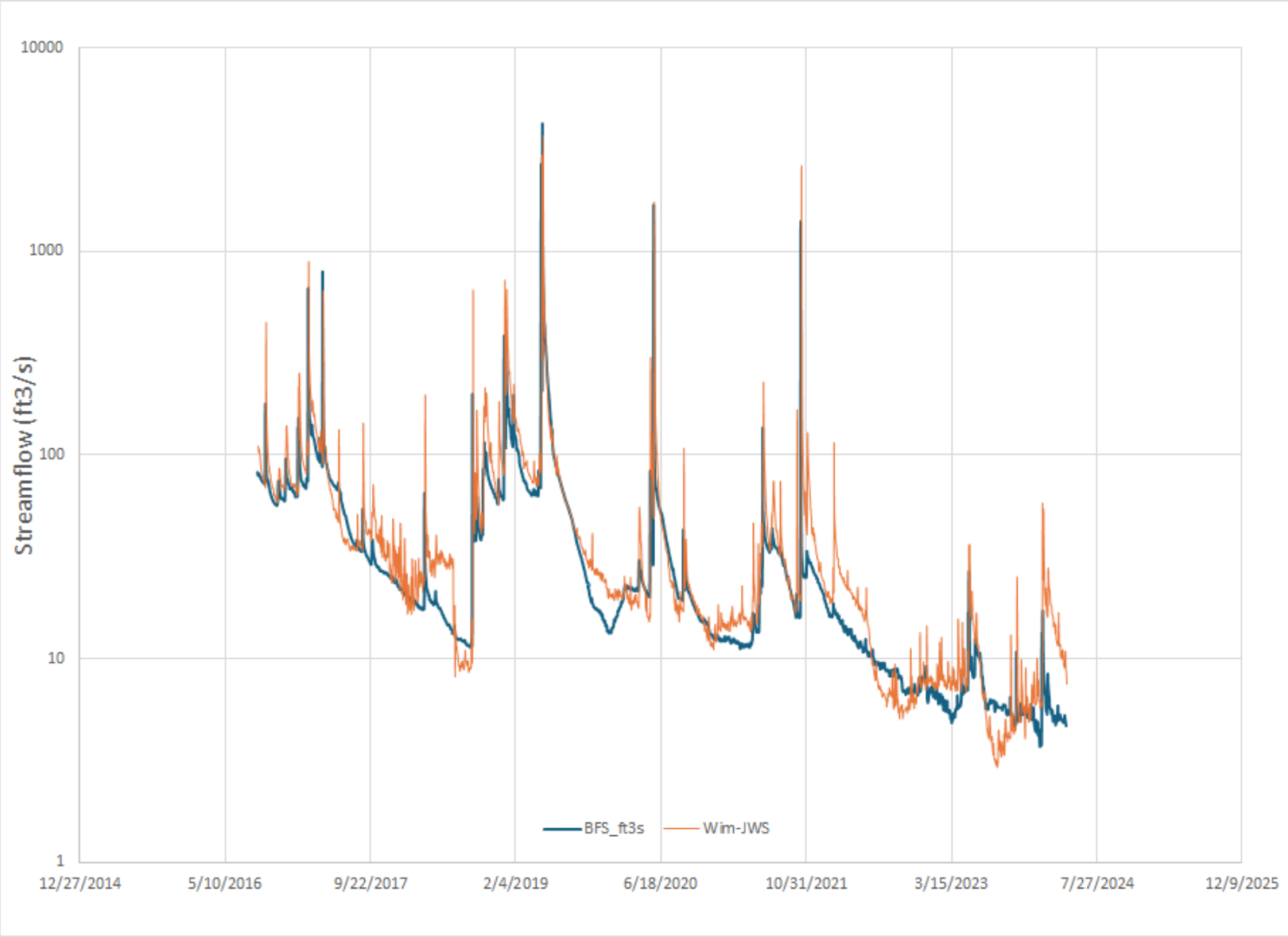

Figure 6. Streamflow hydrographs for Blanco River at Fischer Store Road and at Wimberley. Data from USGS.

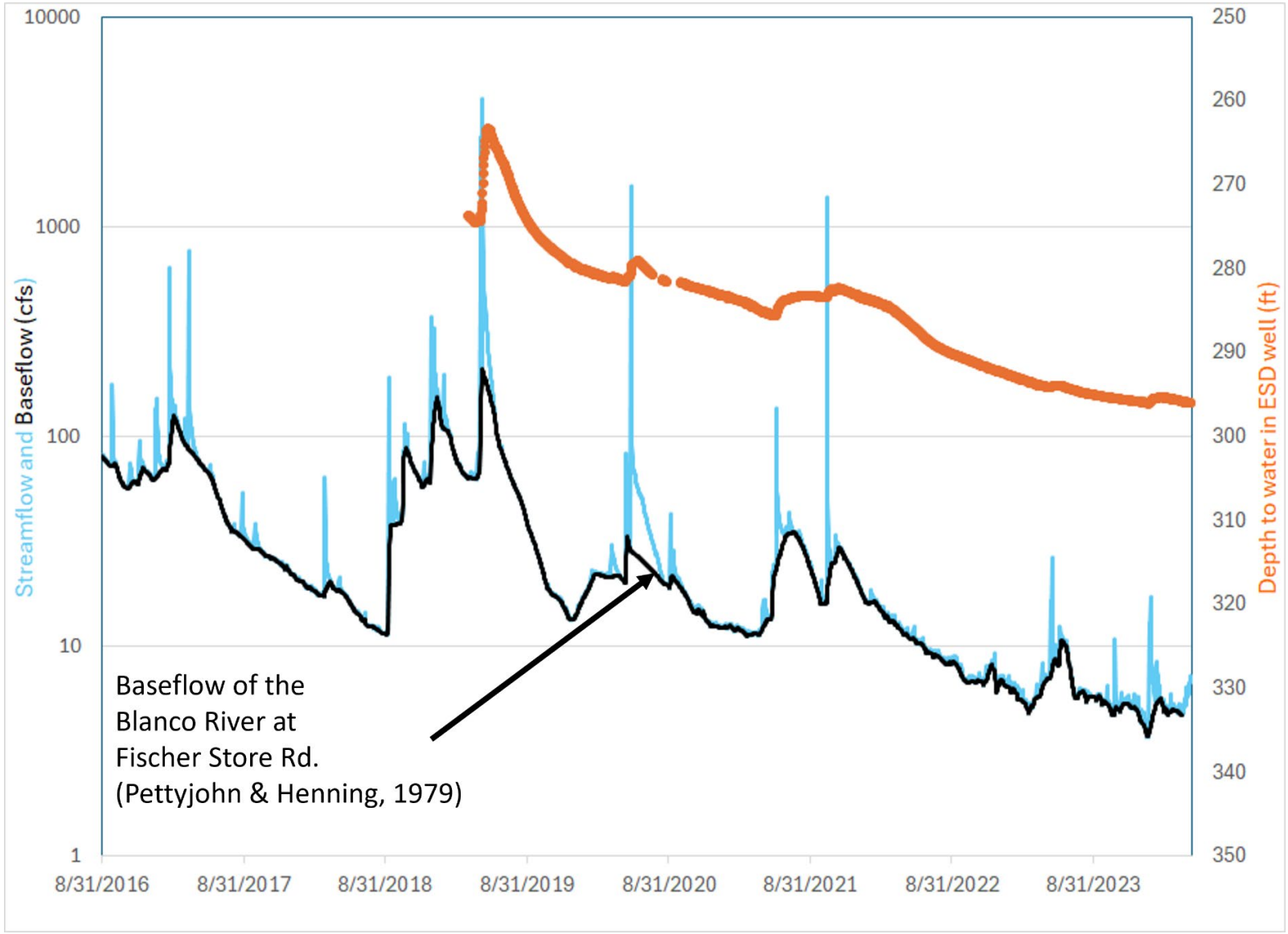

Figure 7. Comparison of Blanco River streamflow at Fischer Store Road and water level readings in the ESD monitor well. The computed Blanco River baseflow curve is shown in black.

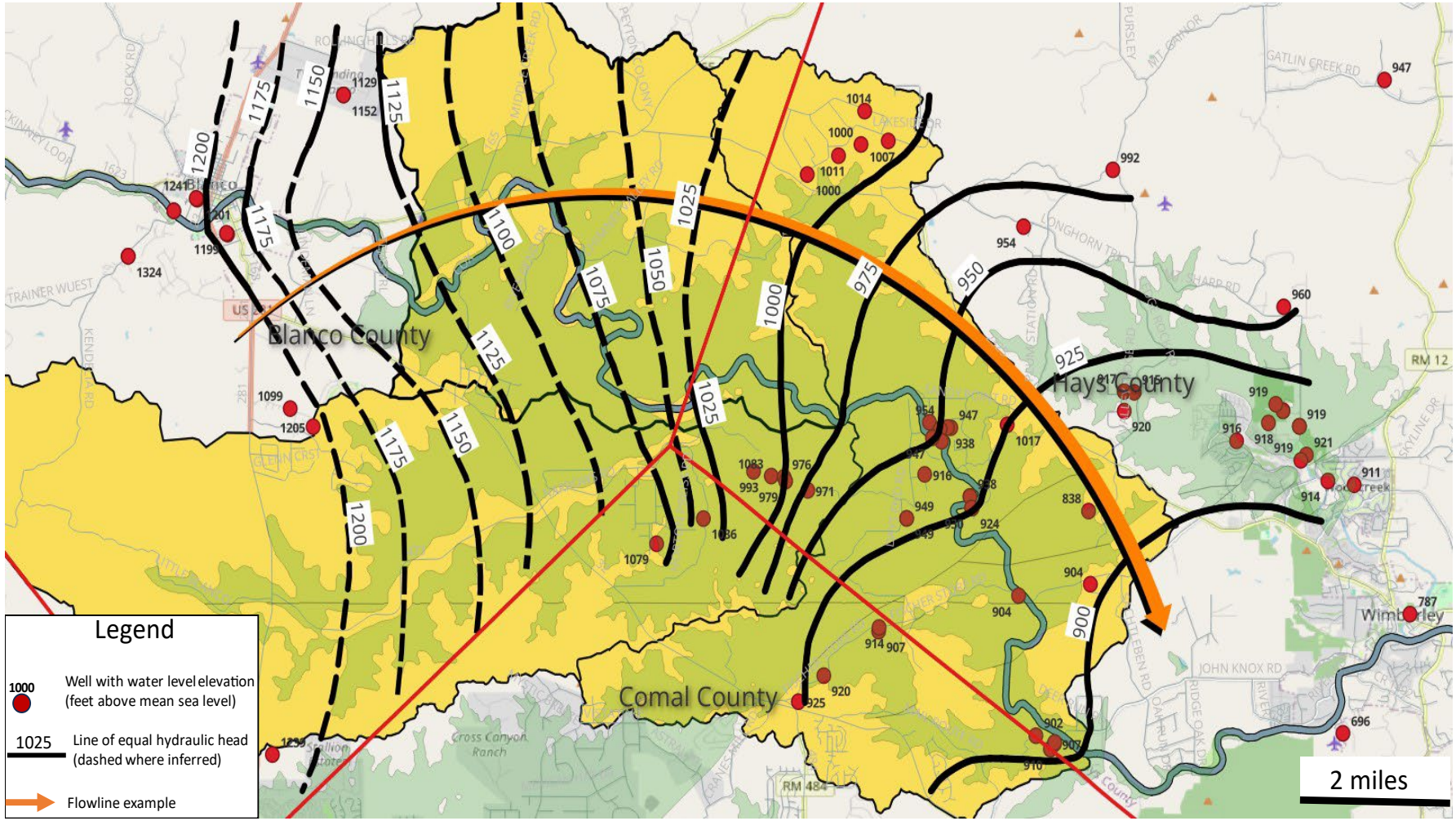

Figure 8. Potentiometric surface map for the Middle Trinity Aquifer in the study area. Data is from Fall 2023 and are shown in Appendix A.

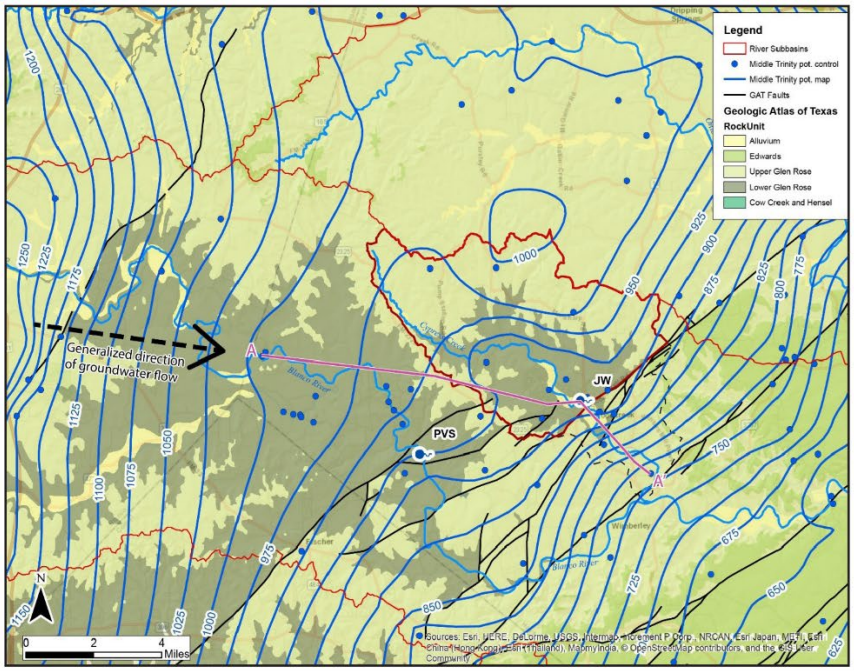

From Hunt et al. (2019)

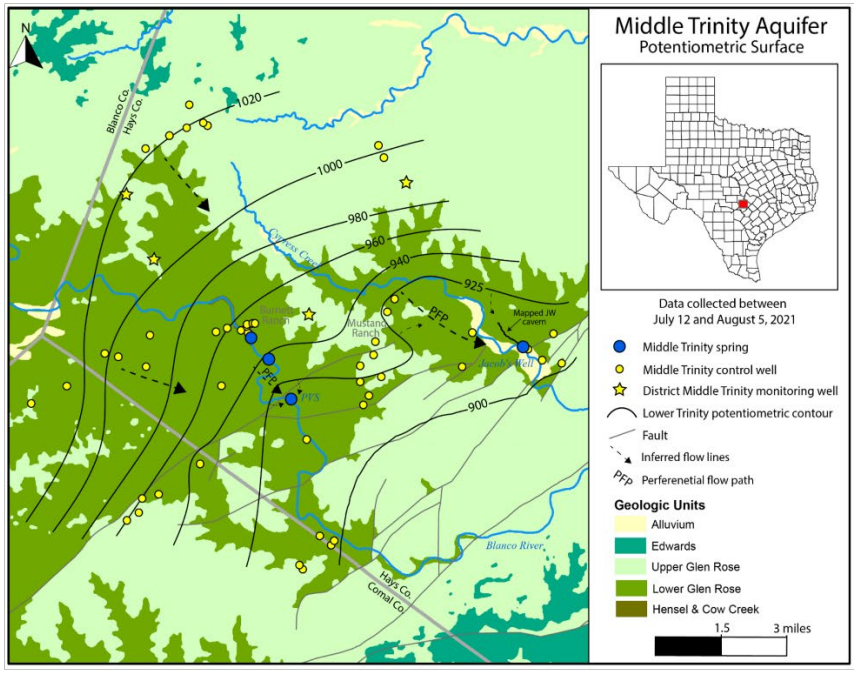

From Heath et al. (2022)

Figure 9. Past potentiometric surface maps in the general area.

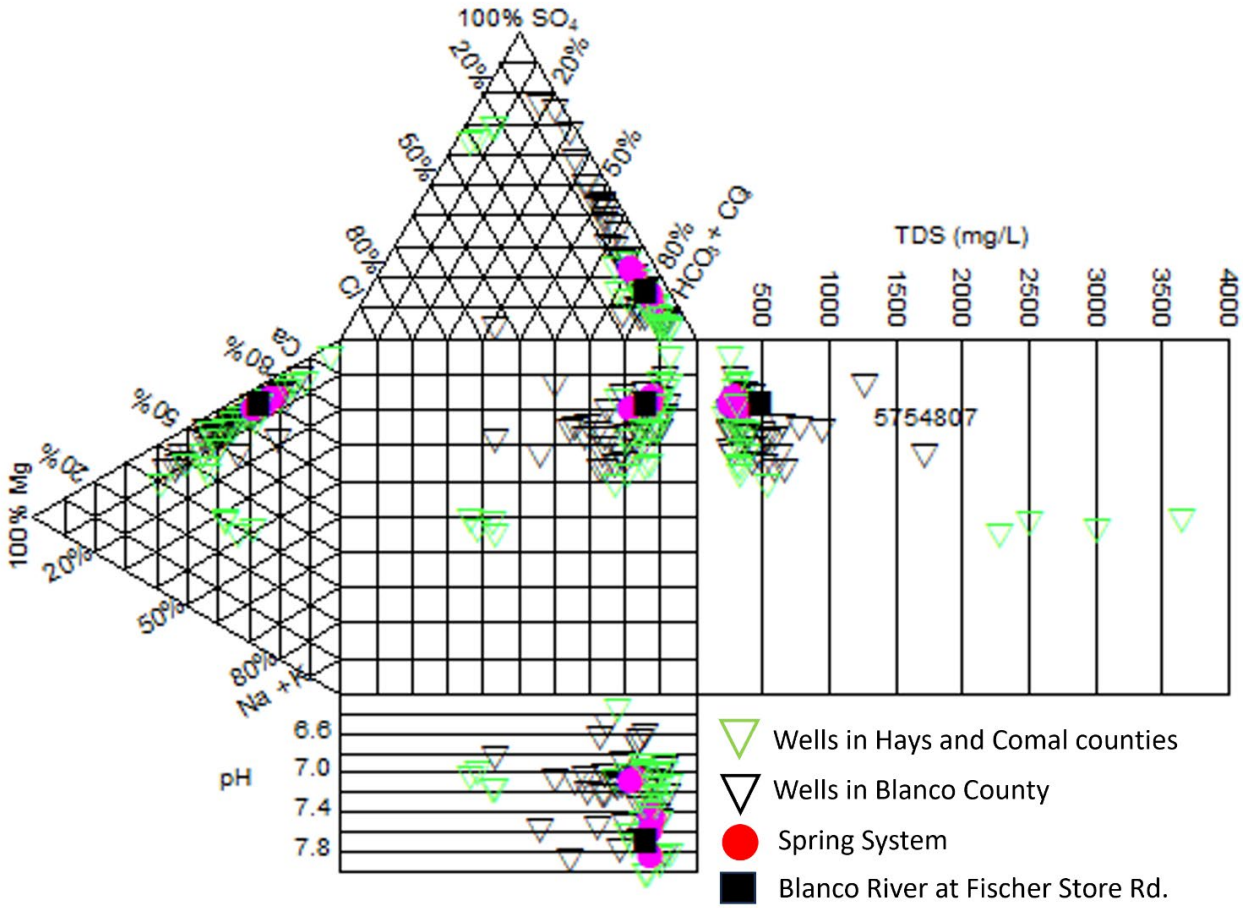

Figure 10. Durov plot of the chemical composition of groundwater, springs, and river in the study area. Data are of various vintages and are shown in Appendix B.

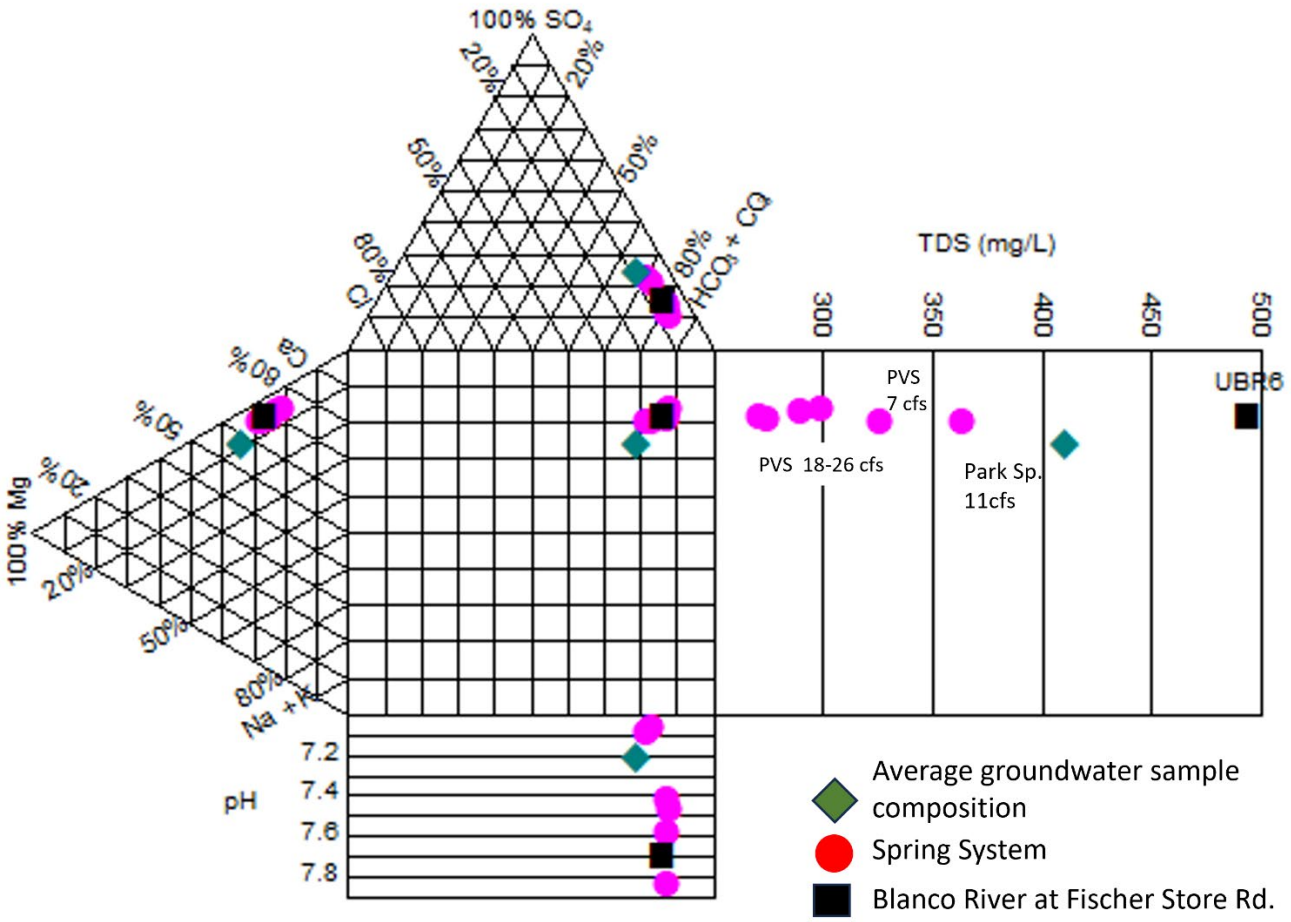

Figure 11. Simplified Durov diagram showing only the general chemistry of springs, Blanco River, and the "average sample"

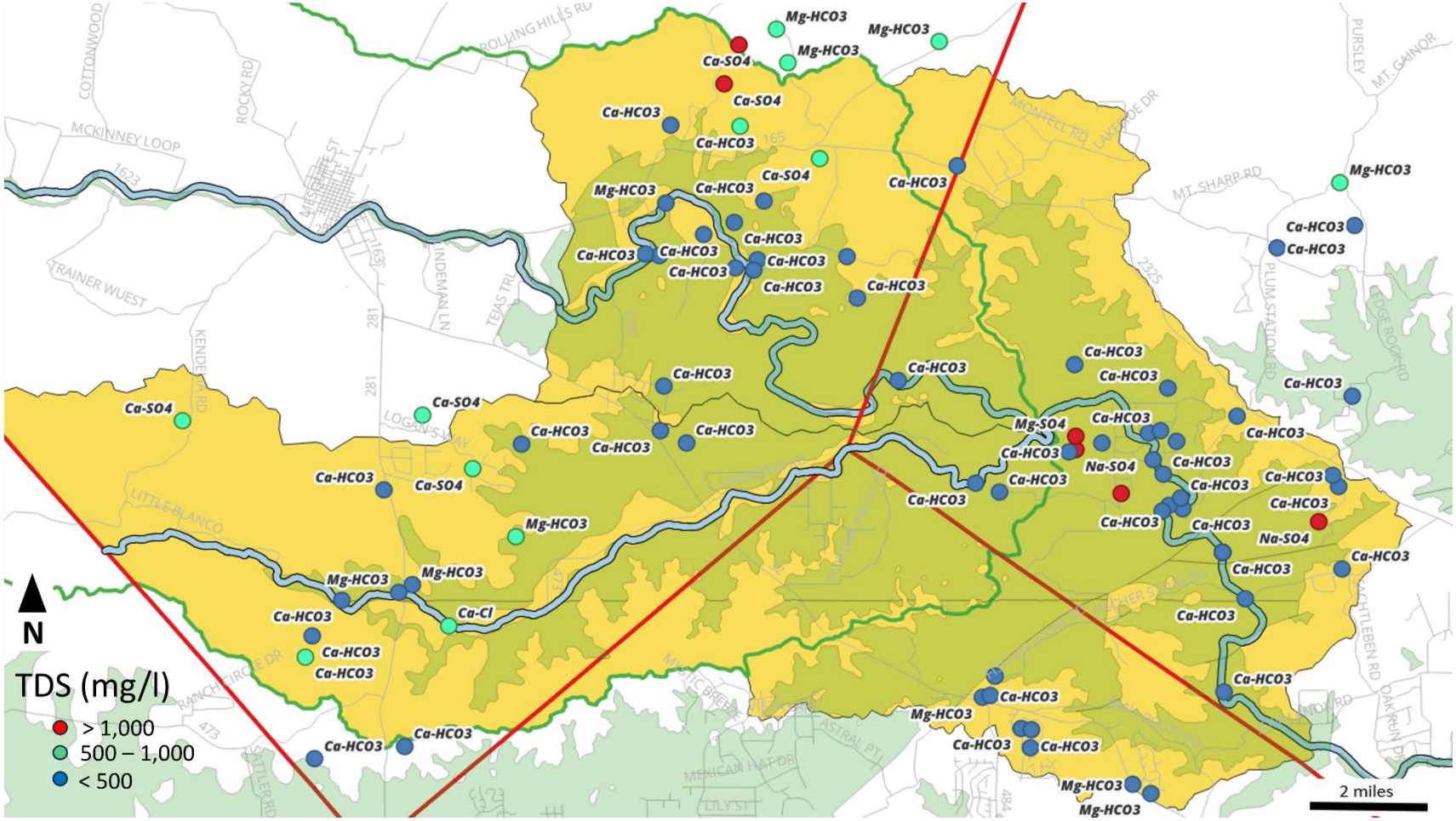

Figure 12. Hydrochemical facies map of groundwater in the Study area.

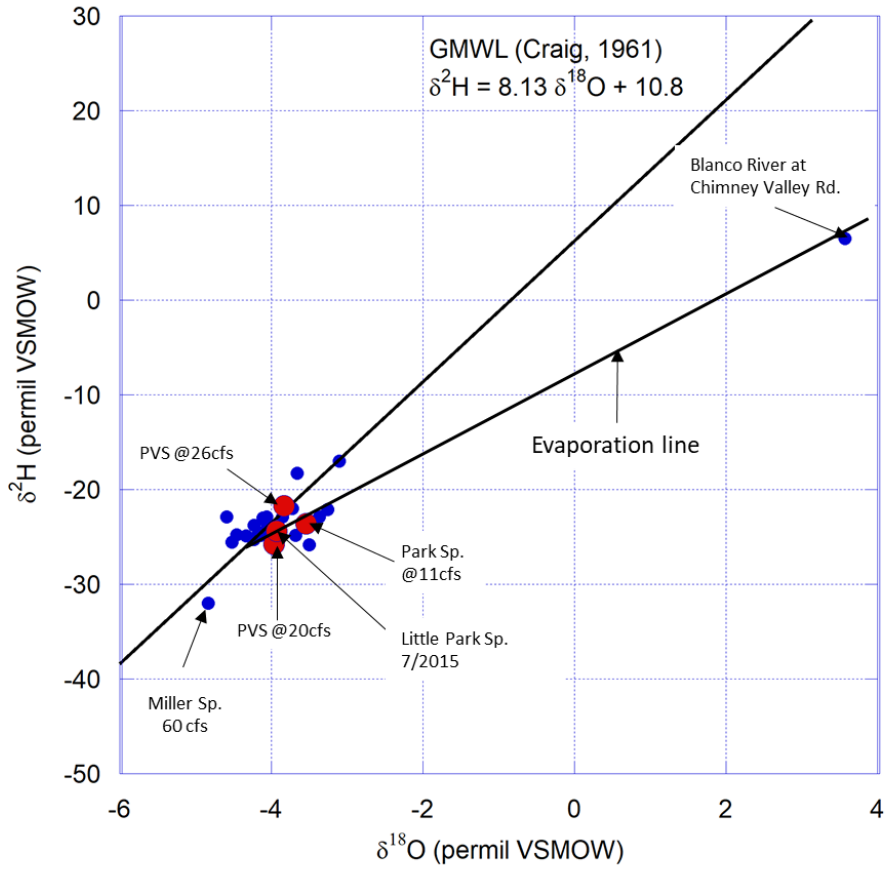

Figure 13. Plot of deuterium vs. oxygen-18 showing meteoric origin and evaporation processes for groundwater in the study area.

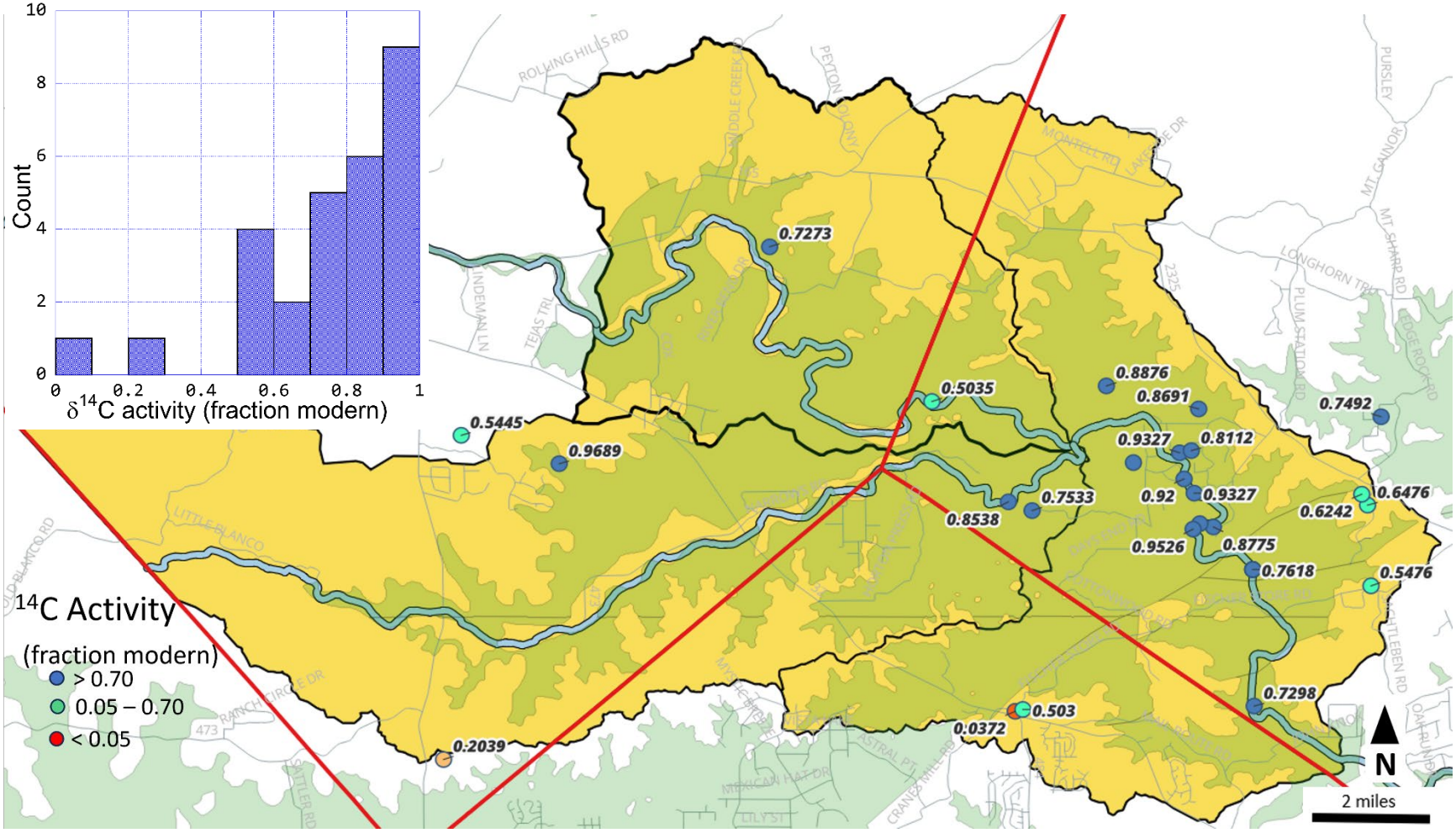

Figure 14. Carbon-14 activities for groundwater and spring water samples in the study area. The histogram (inset) shows most of the samples are indicative of active recharge processes.

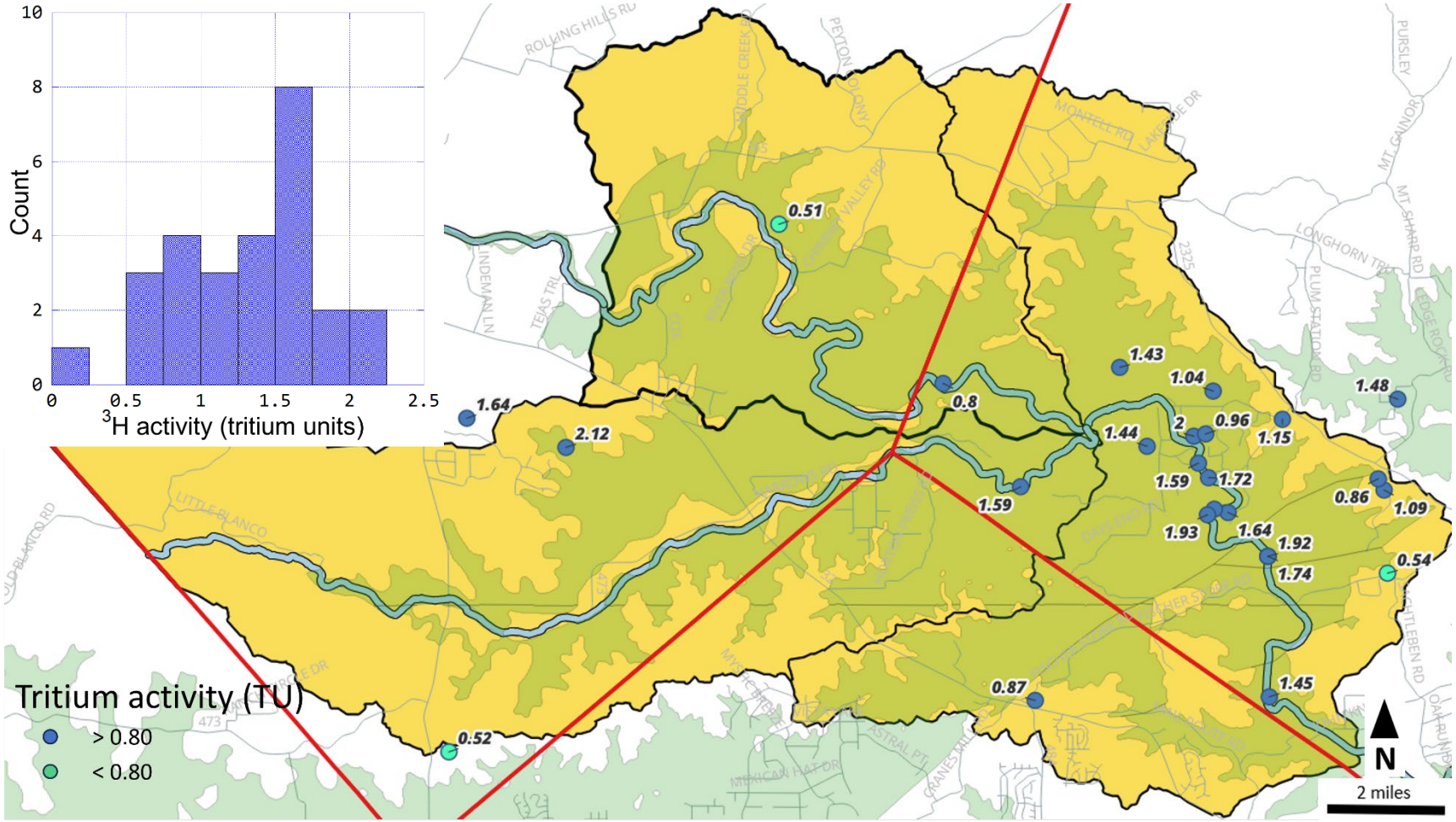

Figure 15. Tritium activities for groundwater and spring water samples in the study area. The histogram (inset) shows most of the samples have received modern recharge.

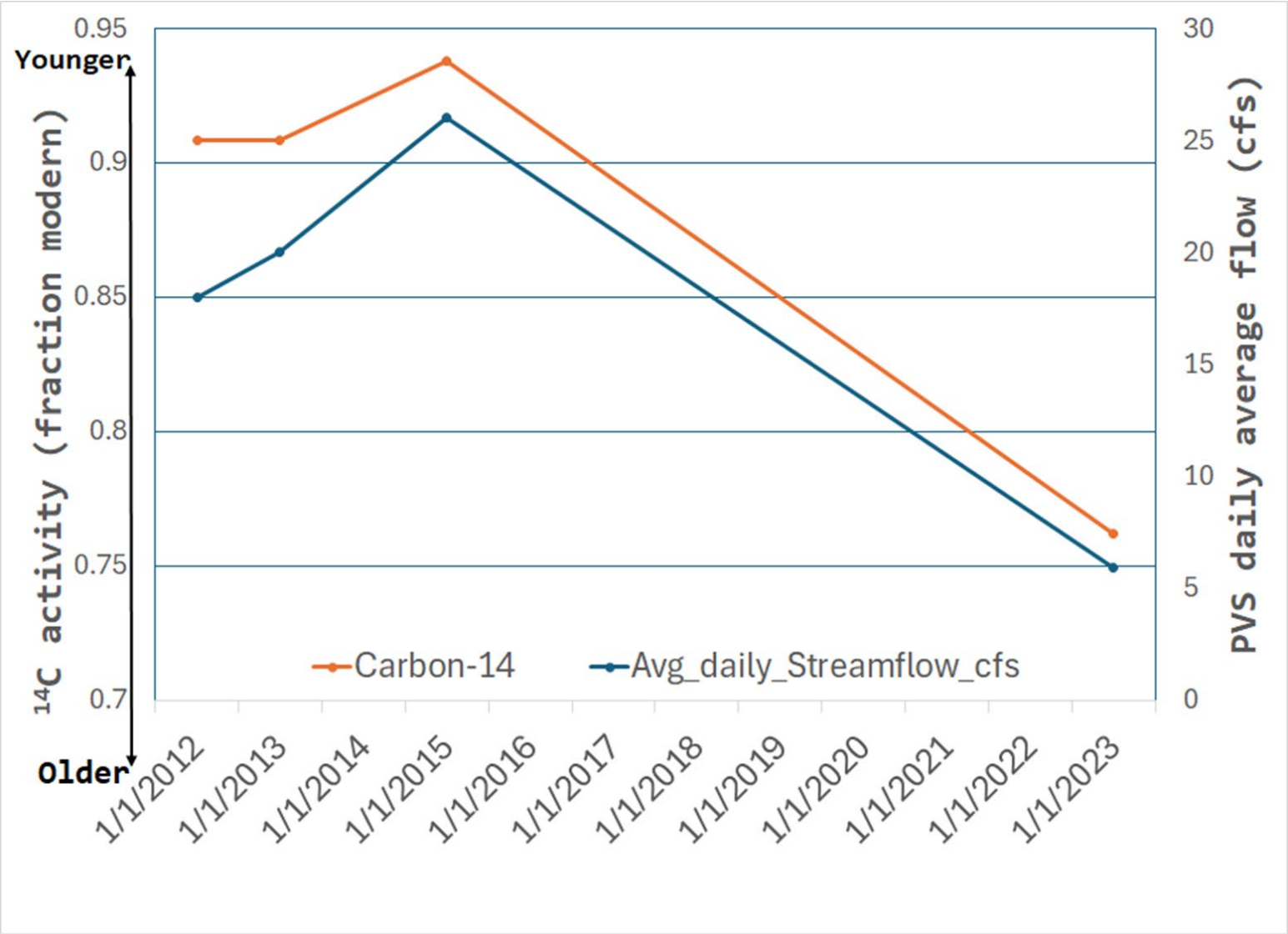

Figure 16. Chart showing the correlation between springflow at PVS and carbon-14 activities in spring samples.

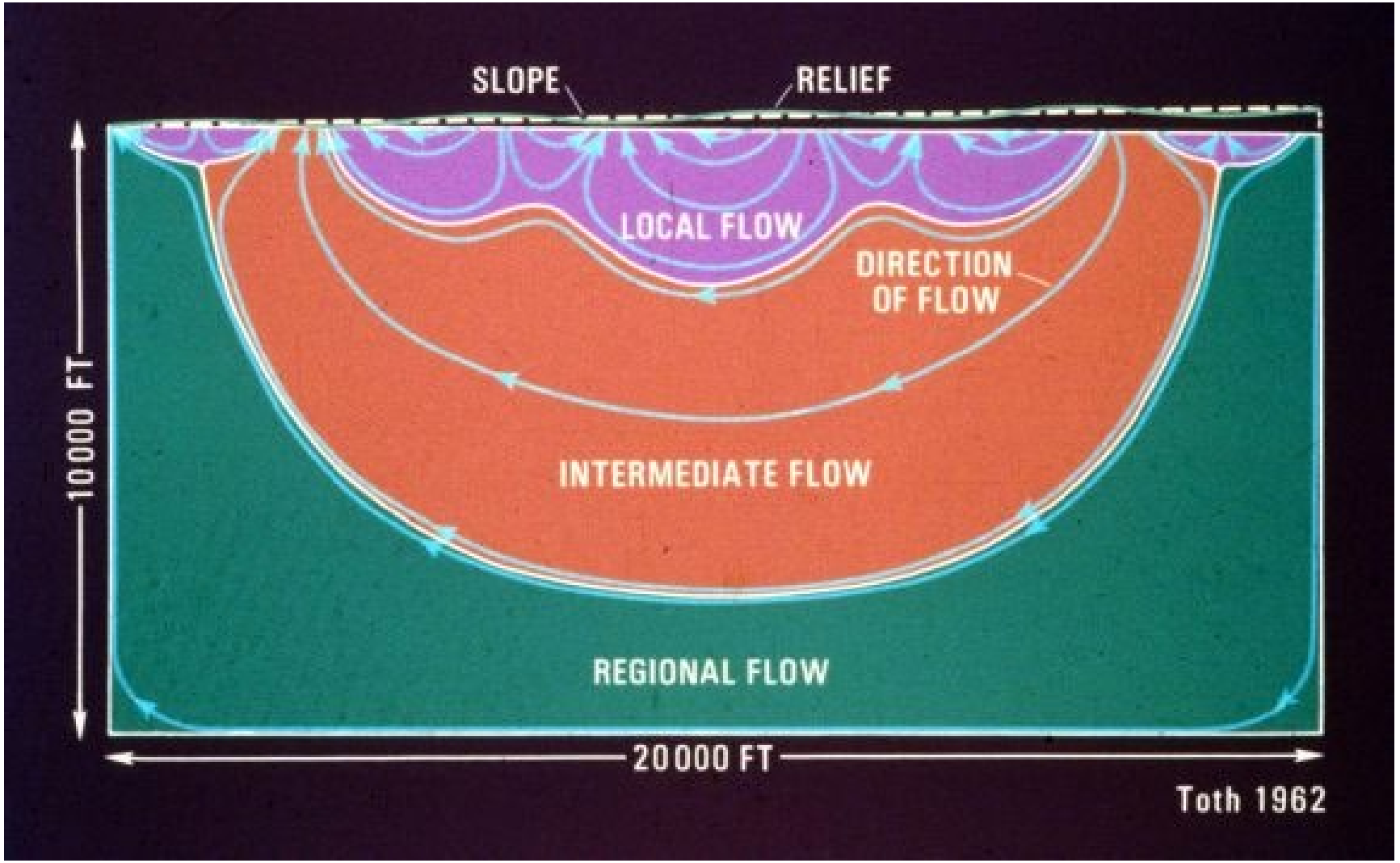

Figure 17. Schematic diagram showing theoretical relationships between local, intermediate and regional flow systems.

Baseflow Separation

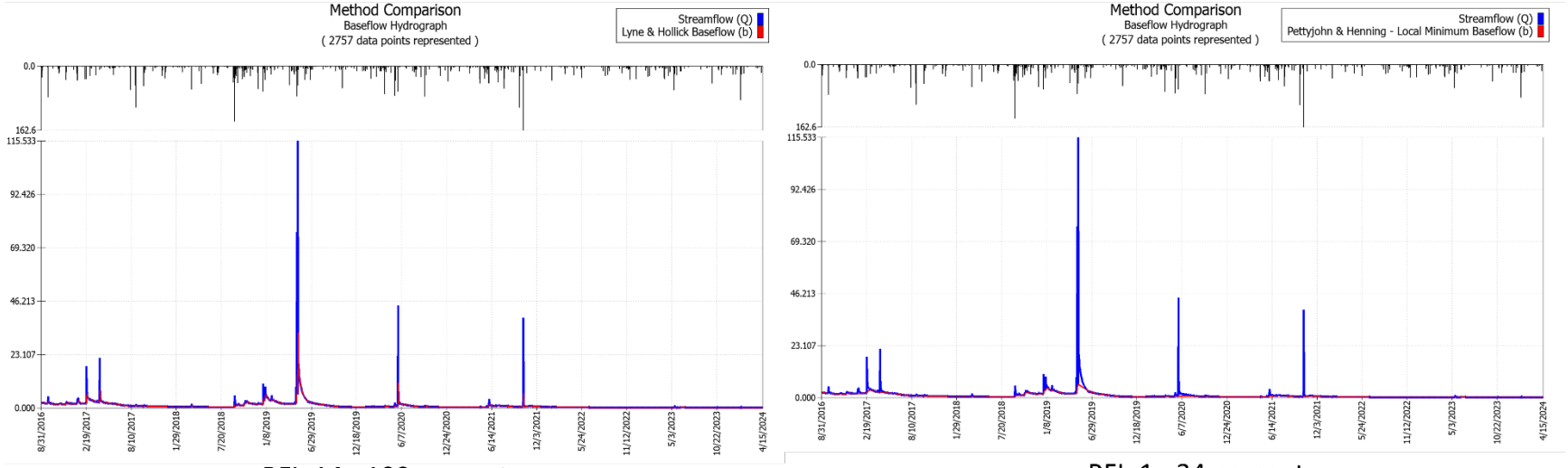

BFI: 14 - 100 percent

Streamflows > 500 cfs

BFI: 1 - 34 percent

Figure 18. Baseflow separation methods applied to Blanco River flows: comparing the results provided by two algorithms.

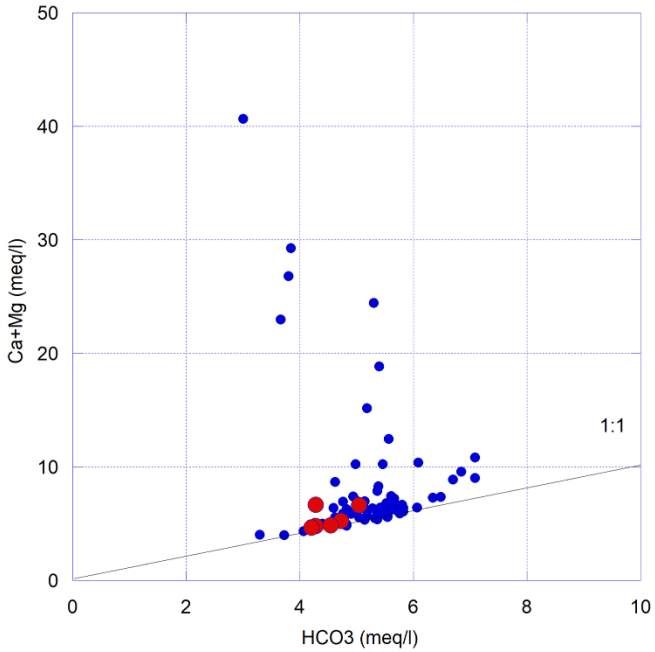

Calcite and dolomite dissolution

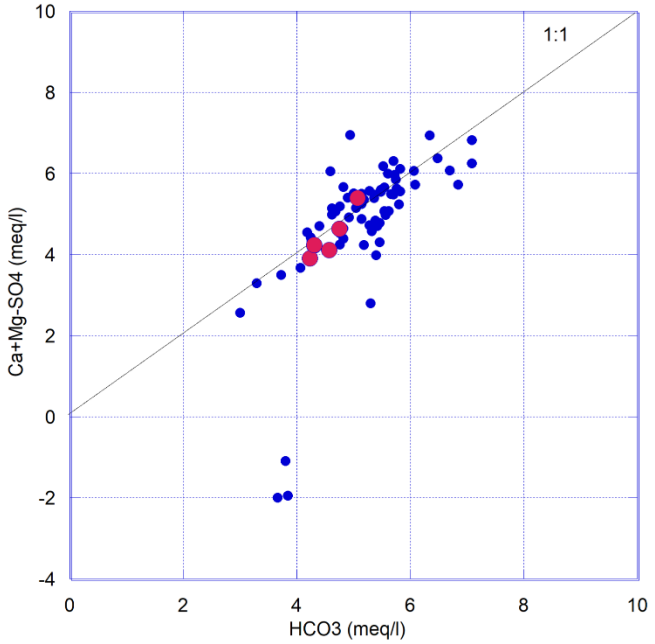

Calcite, dolomite, and gypsum dissolution

Figure 19. Geochemical processes that explain the groundwater and spring composition in the study area.

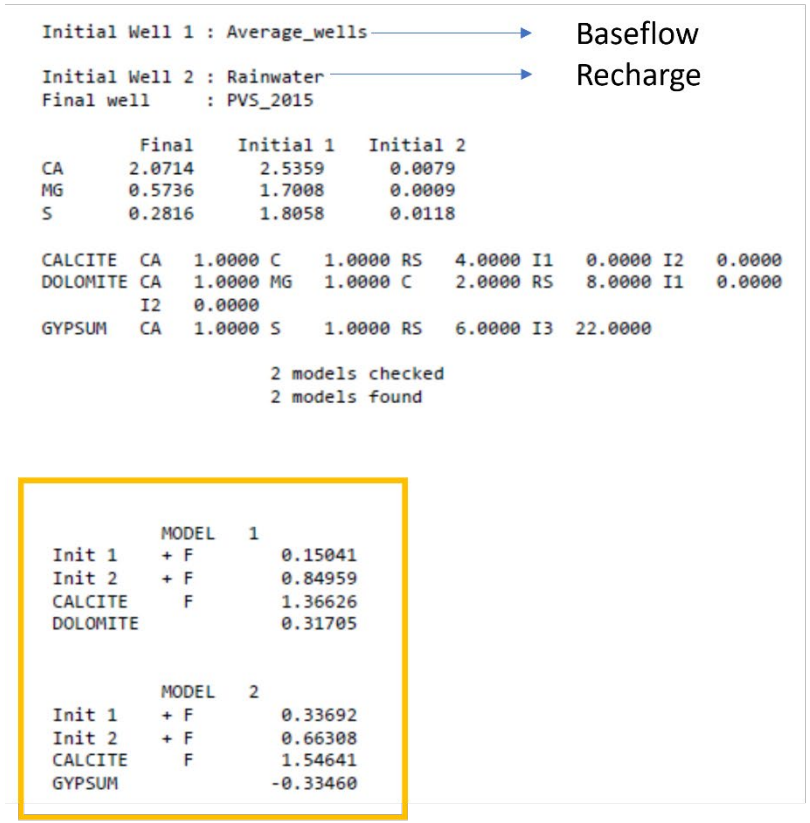

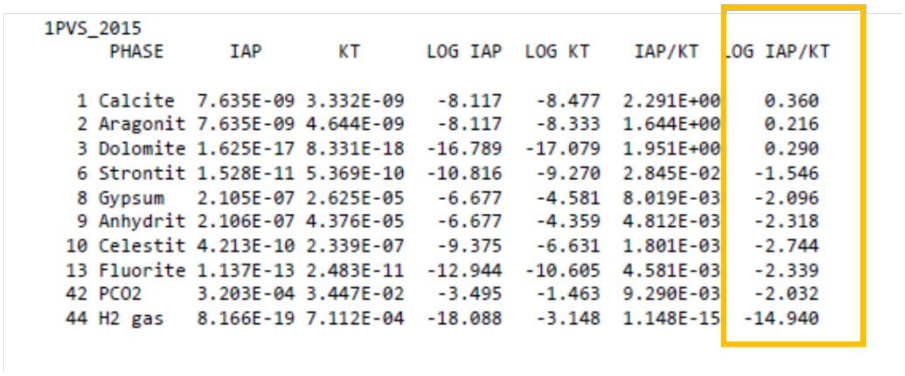

1PVS_2015

	PHASE	IAP	KT	LOG IAP	LOG KT	IAP/KT	LOG IAP/KT
1	Calcite	7.635E-09	3.332E-09	-8.117	-8.477	2.291E+00	0.360
2	Aragonit	7.635E-09	4.644E-09	-8.117	-8.333	1.644E+00	0.216
3	Dolomite	1.625E-17	8.331E-18	-16.789	-17.079	1.951E+00	0.290
6	Strontit	1.528E-11	5.369E-10	-10.816	-9.270	2.845E-02	-1.546
8	Gypsum	2.105E-07	2.625E-05	-6.677	-4.581	8.019E-03	-2.096
9	Anhydrit	2.106E-07	4.376E-05	-6.677	-4.359	4.812E-03	-2.318
10	Celestit	4.213E-10	2.339E-07	-9.375	-6.631	1.801E-03	-2.744
13	Fluorite	1.137E-13	2.483E-11	-12.944	-10.605	4.581E-03	-2.339
42	PCO2	3.203E-04	3.447E-02	-3.495	-1.463	9.290E-03	-2.032
44	H2 gas	8.166E-19	7.112E-04	-18.088	-3.148	1.148E-15	-14.940

Figure 20. NETPATH modeling inputs and outputs: the wet year example.

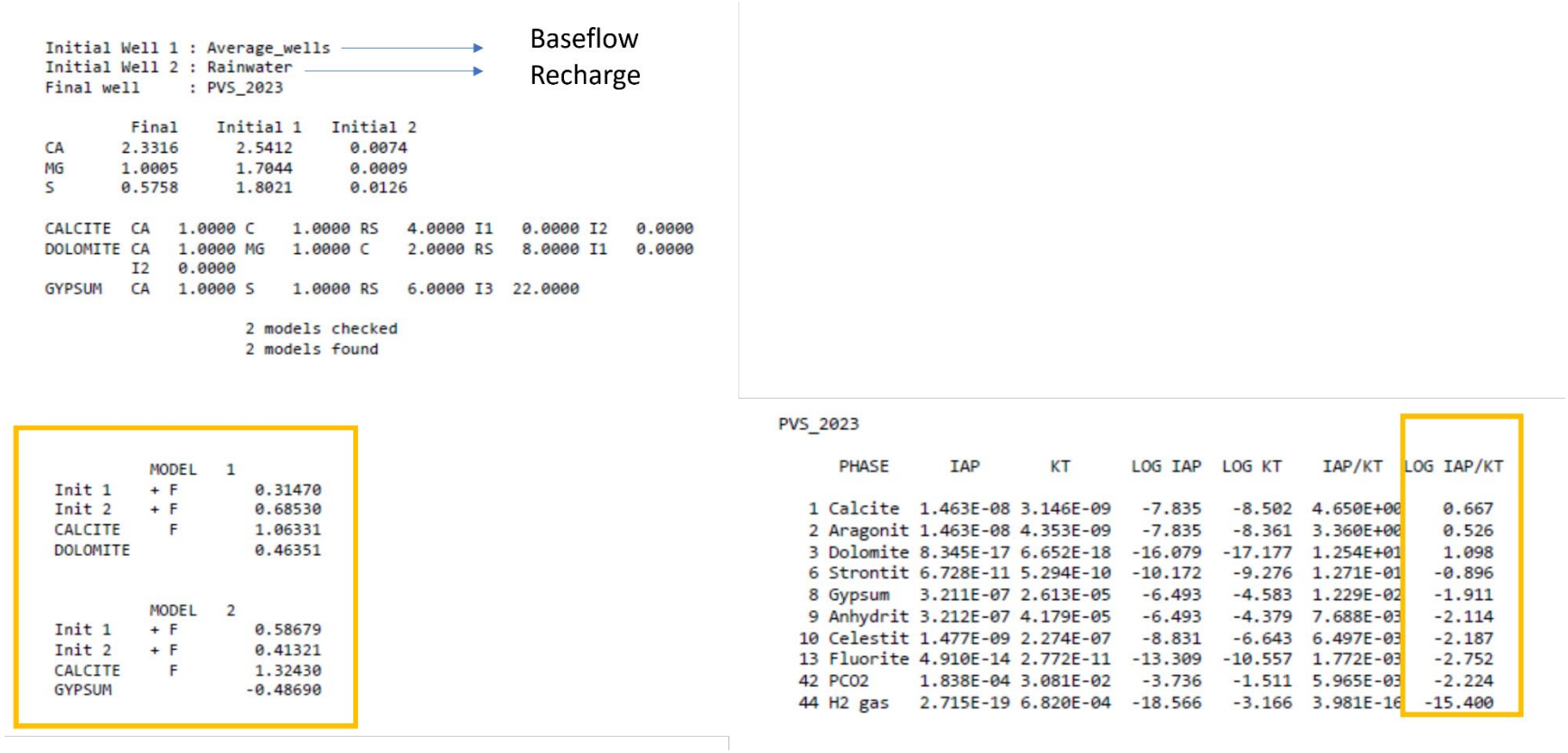

Figure 21. NETPATH modeling inputs and outputs: the dry year example.

Appendix A Water Level Elevation Data

Source	SWN	Ddlat	Ddlong	Aquifer	Date	Depth to Water (ft)	WL elevation (ft)
BPGCD	5761311	30.12228	-98.386140	Middle Trinity	9/15/2023	219.4	1128.6
HTGCD		30.11039	-98.245600	Middle Trinity (LGR-CC	9/23/2023	275.3	999.65
BSEACD	5764723	30.03578	-98.124640	Middle Trinity (CC)	9/6/2023	65.98	921.16
BPGCD		30.08883	-98.417610	Middle Trinity	9/15/2023	147.6	1187.4
UT_MG	5763608	30.047959	-98.132953	Middle trinity	9/26/2023	135.23	918.89
BSEACD		30.07137	-98.130800	Middle Trinity	9/5/2023	314.65	959.78
UT_MG	6808111	29.997528	-98.096519	Middle Trinity	9/27/2023	56.01	787.31
UT_MG		29.965086	-98.194172	Middle Trinity	9/26/2023	49.8	910.16
HTGCD	5764714	30.029533	-98.118811	Middle Trinity	9/14/2023	44.3	913.7
HTGCD		30.04232	-98.221200	Middle Trinity	9/23/2023	109.22	947.16
BPGCD	5761217	30.09444	-98.432220	Middle Trinity	9/15/2023	155	1166
BPGCD	5761223	30.097222	-98.425833	Middle Trinity	9/15/2023	139.5	1200.5
UT_MG	5763611	30.042637	-98.126543	Middle trinity	9/26/2023	151.01	923.47
HTGCD		30.02053	-98.233200	Middle Trinity	9/23/2023	166.6	948.95
HTGCD		30.02053	-98.233200	Middle Trinity	9/23/2023	166.6	948.95
HTGCD		30.04632	-98.174100	Middle Trinity (?)	9/23/2023	284.21	919.59
HTGCD		30.02229	-98.183800	Lower Trinity	9/23/2023	281.3	838.3
HTGCD		30.10317	-98.260200	Middle Trinity (CC?)	9/23/2023	275.65	999.55
HTGCD		30.00472	-98.183300	Lower Trinity	9/23/2023	210.2	904
HTGCD		29.97649	-98.262600	Middle Trinity	9/23/2023	278.35	924.85
BSEACD	5763607	30.043472	-98.134955	Middle Trinity (CC)	9/28/2023	103.85	917.86
HTGCD		29.96889	-98.114720	Middle Trinity	9/14/2023	383.74	696.26
UT_MG	5763708	30.022978	-98.215428	Middle Trinity	9/27/2023	103.52	924.28
HTGCD		30.05083	-98.171400	Middle Trinity (CC?)	9/23/2023	203.5	914.95
BSEACD		30.051034	-98.174142	Middle Trinity (CC)	9/5/2023	243.2	917.31
HTGCD		30.04239	-98.222100	Middle Trinity	9/23/2023	105.2	938.45
UT_MG	6807201	29.966389	-98.193056	Middle Trinity	9/26/2023	55.17	906.97
BSEACD	5763611	30.042675	-98.126542	Middle Trinity	8/31/2023	156.26	918.64
HTGCD		30.04303	-98.205900	Middle Trinity	9/23/2023	199.2	1017.27

Source	SWN	Ddlat	Ddlong	Aquifer	Date	Depth to W	WL elevation (ft)
HTGCD		30.00195	-98.202800	Middle Trinity	9/23/2023	90.9	904.1
HTGCD		30.01444	-98.301100	Middle Trinity	9/23/2023	171.6	1078.53
HTGCD	5756710	30.125872	-98.103433	Middle Trinity	9/14/2023	247.92	947.08
HTGCD		29.96669	-98.193000	Middle Trinity (LGR)	9/23/2023	56.61	905.48
HTGCD		30.04363	-98.227000	Middle Trinity	9/23/2023	85.64	954.36
HTGCD		30.02575	-98.216000	Middle Trinity (CC?)	9/23/2023	73.92	937.88
HTGCD		30.02306	-98.215600	Middle Trinity (CC?)	9/23/2023	99.92	929.88
HTGCD		30.03111	-98.228300	Middle Trinity (CC?)	9/23/2023	175.65	915.85
HTGCD		30.04199	-98.224100	Middle Trinity	9/23/2023	61.87	948.53
HTGCD		30.1184	-98.244600	Middle Trinity (CC)	9/23/2023	334.5	1013.7
HTGCD	5763205	30.09063	-98.201450	Middle Trinity	9/14/2023	393.3	953.7
HTGCD		29.98275	-98.255700	Middle Trinity (CC?)	9/23/2023	187.8	919.7
HTGCD		29.96832	-98.198100	Middle Trinity	9/23/2023	76.8	901.8
BPGCD	5761624	30.04255	-98.394390	Middle Trinity	9/15/2023	233	1205
BPGCD		30.04692	-98.400610	Middle Trinity	9/15/2023	286.4	1098.6
BPGCD	5761507	30.083528	-98.444611	Middle Trinity	9/15/2023	99.2	1323.8
HTGCD		30.11124	-98.238200	Middle Trinity (LGR?)	9/23/2023	277.8	1006.85
HTGCD		30.03907	-98.223700	Middle Trinity	9/23/2023	69.88	953.67
HTGCD		30.02049	-98.288400	Middle Trinity	9/23/2023	130.8	1036.25
HTGCD		30.0399	-98.226200	Middle Trinity	9/23/2023	79.53	947.23
HTGCD		30.10429	-98.177200	Middle Trinity (CC)	9/23/2023	385.7	991.5
BSEACD		30.030439	-98.266486	Middle Trinity (CC)	9/5/2023	102.65	976.28
BSEACD		30.027263	-98.260026	Middle Trinity (CC)	9/5/2023	151.72	971.21
BSEACD	5762902	30.02948	-98.266050	Middle Trinity(CC)	9/5/2023	94.14	978.81
BSEACD		30.031831	-98.274776	Middle Trinity	9/5/2023	97.6	993.47
HTGCD		30.02861	-98.111667	Middle Trinity	9/15/2023	53.24	910.76
HTGCD		30.10769	-98.251700	Middle Trinity (?)	9/23/2023	294.7	1010.65
HTGCD	5763908	30.039166	-98.143610	Middle Trinity (CC)	9/15/2023	133.64	916.36
HTGCD		29.99343	-98.240800	Middle Trinity	9/23/2023	235.5	906.75
HTGCD		29.99433	-98.240700	Middle Trinity	9/23/2023	231.2	913.8

Appendix B Water Quality and Isotope Data

Sample ID	Latitude	Longitude	Date	Temperat	Calcium	Magnesiu	Sodium	Potassiun	Strontium	Carbonat	Bicarbona	Sulfate	Chloride	Fluoride	Nitrate	pH	Dissolved	Aquifer	Carbon-14	Carbon-13	Deuteriur	Oxygen-1	Tritium
				°C	mg/L	mg/L	mg/L	mg/L	mg/L	mg/L	mg/L	mg/L	mg/L	mg/L	mg/L	pH_SU	mg/L		Fmdn	PDB	permil	permil	TU
5754806	30.1425	-98.3147	6/1/1996	22	85	80	15	10	32	0	432	220	14	3	0.35	7	682	Trinity					
5754807	30.12889	-98.3275	8/1/2013	22.4	249	146	48.7	16.3	15.5	0	323.4	1040	49.7	2.12	1.49	7.55	1739	Trinity					
5754808	30.13861	-98.3239	8/1/2014	20.7	304	44.8	8.86	4.65	20.4	0	329.5	714	12.2	1.19	0.21	7.03	1284	Trinity					
5754809	30.13417	-98.3119	7/1/2023	23.1	79.1	68.4	17.3	9.45	26.1	0	417.4	185	14	1.8	0.02	6.6	616.5	Trinity					
5754907	30.13945	-98.275	12/1/1988	24	76.5	61.6	15	8.3	0	0	408.7	135	22	1	0.49	7.1	526	Trinity					
5761407	30.045	-98.4597	7/1/2016	0	168	82.4	7.27	4.9	3.73	0	316.1	525	7.25	1.04	2.183	7.84	968.3	Trinity					
5761620	30.04639	-98.4011	8/1/2006	22.7	154	58.1	16.1	4.1	4.84	0	339.3	360	19	0.6	0.44	7.06	795	Trinity	0.5445	-7.4			1.64
5761803	30.00028	-98.4208	6/1/1994	22.9	78	33	9.5	1.8	2.41	0	349	31	13	0.72	0.22	7.03	354	Trinity					
5761904	30.02778	-98.4106	6/1/1994	24.2	71	38	7.8	2.9	2.39	0	353.9	69	13	2.49	0.26	7.02	392	Trinity					
5761912	30.03917	-98.3769	5/1/2005	20.5	99.2	8.82	5.21	0.79	0.477	0	316.1	15.6	7.69	0.26	1.01	6.91	309	Trinity	0.9689	-7.7	-17	-3.1	2.12
5761913	30.01611	-98.3783	8/1/2009	21.9	93	69.5	12.4	5.7	32.8	0	371	223	12.3	3.15	0.22	7.19	646	Trinity					
5761914	30.00417	-98.4036	7/1/2016	0	61.5	41.3	11.1	2.78	53.4	0	333.2	104	20.9	2.61	0.02	7.76	473.4	Trinity					
5761915	30.03306	-98.3889	7/1/2012	23	129	46.1	13.6	3.28	4.62	0	333.1	262	17.9	0.63	2.46	7.17	655	Trinity					
5761917	30.00222	-98.4069	6/1/2014	20.9	57.3	43.5	11.5	2.58	40.3	0	330.7	83.7	20.5	2.4	0.09	7.49	437	Trinity					
5762110	30.08611	-98.3433	8/1/2005	21	91.7	22.5	6.1	0.62	3.1	0	369.8	17.5	9.41	0.32	2	7.18	350	Trinity					
5762111	30.11861	-98.3406	8/1/2009	21.7	107	16.8	7.1	1.1	4.37	0	338	51.4	12.3	0.37	1.22	7.31	379	Trinity					
5762117	30.08653	-98.3468	7/1/2020	32.9	69	29.8	8.26	1.65	7.16	0	290.4	34	13	0.264	2.678	6.69	321.5	Trinity					
5762203	30.09972	-98.3178	7/1/2020	23.8	102	23.3	9.77	1.6	0.927	0	305.1	72.1	14.9	0.218	1.877	6.47	387.8	Trinity					
5762212	30.11028	-98.3042	8/1/2022	23	120	51.7	18	3.38	6.42	0	303.9	232	16.4	0.693	0.146	7.02	610.3	Trinity					
5762213	30.09139	-98.3325	8/1/2009	21.9	55.4	26.3	12.5	1.8	1.55	0	255.1	18.7	19.9	0.28	5.8	7.66	279	Trinity					
5762214	30.11833	-98.3236	8/1/2009	22	106	41.1	14.4	2.6	2.96	0	281.9	177	17.2	0.39	2.35	7.52	514	Trinity					
5762215	30.08586	-98.2975	6/1/2020	22.1	90.6	12.8	10.9	1.25	3.96	0	307.5	20.4	17.7	0.361	8.633	7.13	327.8	Trinity					
5762216	30.08508	-98.3194	7/1/2020	21.9	82	21.5	9.69	0.991	0.264	0	299	22	15.9	0.191	1.116	6.68	311.7	Trinity					
5762218	30.09439	-98.325	7/1/2020	22.4	66.4	27.1	7.9	1.6	0.777	0	281.9	19.3	13.2	0.241	4.604	6.64	292.2	Trinity	0.7273	-5.9	-21.98	-3.72	0.51
5762302	30.1085	-98.2706	8/1/1996	24	75	39	13	3.8	0	0	290.4	130	15	0.6	0.55	7	431	Trinity					
5762411	30.05361	-98.3422	7/1/2017	0	102	34	9.15	1.97	3.02	0	327.1	120	10.5	0.44	3.055	7.12	455.9	Trinity					
5762413	30.0425	-98.3431	7/1/2005	22.3	89.7	16.7	5.98	0.73	4.76	0	327.1	17.7	10.3	0.47	5.97	6.98	326	Trinity					
5762503	30.0825	-98.3203	10/1/1988	21	61.6	23.6	9	1.4	0	0	268.4	15	12	0.3	4.16	7.4	264	Trinity					
5762508	30.08306	-98.3247	6/1/1994	22.8	59	23	18	2.7	1.55	0	258.7	20	27	0.32	2.61	7.09	292	Trinity					
5762509	30.07556	-98.295	7/1/2014	22	68.3	18.9	6.46	1.5	1	0	294.1	15.3	9.82	0.36	8.68	7.81	289	Trinity					
5762603	30.055	-98.285	6/1/2013	23.93	57	24	5.23	1.27	0.5	0	294.1	20.4	9.68	0.27	2.97	7.45	277	Trinity	0.5035	-14.6	-24.9	-4.33	0.8
5762709	30.03945	-98.3367	7/1/2010	21.8	73.6	31.6	10.4	1.54	24.5	0	342.9	57.5	14.4	0.58	0.89	7.33	397	Trinity					
5762902	30.02944	-98.2661	6/1/2013	23.67	80.5	12.4	7.38	1.33	0.39	0	290.4	24.7	16.3	0.23	2.51	6.33	298	Trinity	0.8538	-13	-22.9	-3.85	1.59
5763201	30.08806	-98.1925	7/1/1996	25	71	34	9.2	2.6	2.3	0	322.2	78	13	0.5	1.25	7	381	Trinity					
5763207	30.09361	-98.1736	2/1/2000	0	75.5	44.5	16.8	3.5	0	0	341.7	68.8	18.2	0.55	0.06	7.7	396	Trinity					
5763208	30.10428	-98.1772	8/1/2023	24.03	62.3	72	21.7	9.51	24.5	0	432	106	32.1	2.48	0.02	7.04	554.2	Trinity					
5763402	30.04194	-98.2239	6/1/2013	25.97	54.2	15.7	5.38	1.48	0.39	0	227	24	10.1	0.2	1.5	7.58	234	Trinity	0.9327	-11.2	-22.1	-3.26	2
5763403	30.05897	-98.2419	6/1/2020	20.9	95.2	19.3	8.05	1.23	0.695	0	322.2	37.1	12.1	0.191	2.572	7.22	345.4	Trinity	0.8876		-24.3	-4.07	1.43

Appendix B Water Quality and Isotope Data-continued

Sample ID	Latitude	Longitude	Date	Temperat	Calcium	Magnesiu	Sodium	Potassiun	Strontium	Carbonat	Bicarbona	Sulfate	Chloride	Fluoride	Nitrate	pH	Dissolved	Aquifer	Carbon-14	Carbon-13	Deuteriur	Oxygen-1	Tritium
				°C	mg/L	mg/L	mg/L	mg/L	mg/L	mg/L	mg/L	mg/L	mg/L	mg/L	mg/L	pH_SU	mg/L		Fmdn	PDB	permil	permil	TU
5763404	30.05311	-98.2192	10/11/2018	21.73	95.9	18.4	7.66	0.865	0.638	0	334.4	33.8	9.73	0.159	3.17	7.3	345.8	Trinity	0.8691	-9.5	-23.5	-4.06	1.04
5763406	30.0425	-98.221	5/1/2023	21.31	85.3	26.1	7.01	1.4	0.374	0	355.1	14.1	10.9	0.15	2.984	6.9	334.2	Trinity	0.8112	-9.7	-24.79	-4.46	0.96
5763503	30.05111	-98.1742	6/1/2013	23.42	75.7	19.1	5.96	1	0.44	0	313.6	22.5	11.3	0.25	2.46	7.19	389	Trinity	0.7492	-11.1	-25.3	-4.23	1.48
5763504	30.04613	-98.2023	8/1/2021	22.17	101	21.4	8.3	1.24	0.532	0	336.8	30	12.1	0.217	2.7	7.19	353.4	Trinity			-23.8	-4.23	1.15
5763701	30.03778	-98.2417	9/1/2004	23.4	318	163	412	21.6	8.55	0	234.3	1500	476	1.14	0.28	6.97	3029	Trinity					
5763702	30.03945	-98.2353	7/1/2020	21.73	115	9.47	9.13	0.749	0.131	0	347.8	10	16.9	0.0917	6.065	7.47	348.2	Trinity	0.8614	-10.2	-23	-4.11	1.44
5763704	30.03722	-98.2433	12/1/1998	27.5	102	1.69	3.67	0.38	0.12	0	285.6	8.28	6.88	0.06	4.24	7.09	277	Trinity					
5763706	30.04111	-98.2417	7/1/2007	23.3	242	179	284	20.7	8.17	0	231.9	1340	314	1.7	3.54	7.14	2520	Trinity					
5763707 (F	30.03167	-98.2203	4/1/2021	21	94.2	23.4	9.13	1.52	1.06	0	307.5	57.5	12.8	0.249	3.125	7.07	364.6	Trinity	0.9327	-13.9	-23.6	-3.57	1.72
5763708	30.02306	-98.2156	6/1/2023	22.21	93.7	22.9	8.39	1.63	0.745	0	305.1	52.4	11.1	0.22	2.723	7	354.8	Trinity	0.8775	-15	-24.8	-3.68	1.64
5763709 (I	30.03528	-98.2228	7/1/2015	25.98	70.1	15.7	7.25	1.46	0.29	0	261.1	25.2	12.5	0.18	2.16	7.42	275	Trinity	0.92	-14.9	-25.8	-3.99	1.59
5763710	30.02389	-98.2189	11/1/2013	20.14	61.7	15.2	5.7	1.52	0.4	0	247.7	31.8	10.1	0.19	1.93	6.95	259	Trinity	0.9373	-13.6	-22.9	-3.37	1.7
5763711	30.0225	-98.2206	7/1/2015	25.38	75.5	15.8	7.63	1.45	0.41	0	259.9	34.9	13.3	0.22	2.34	7.48	291	Trinity	0.9526	-10.1	-32	-4.83	1.93
5763713	30.02687	-98.2306	8/1/2021	25	373	268	406	29.7	13.2	0	183.1	1830	637	1.2	0.02	7.02	3662	Trinity					
5763714	30.03986	-98.2171	8/1/2021	23.45	69.9	18.1	9.41	2.83	0.558	0	280.7	39.2	12.7	0.231	1.607	7.21	302.4	Trinity					
5763715	30.02575	-98.216	6/1/2023	21.34	88.8	22.9	7.92	1.52	0.591	0	313.6	39.4	10.8	0.187	3.201	6.96	340.2	Trinity					
5763806	30.00806	-98.1767	8/1/2021	24.44	89	34.7	10.6	1.88	0.959	0	386.9	17.3	14.9	0.359	0.126	6.98	372.6	Trinity	0.5476	-7.7	-18.29	-3.66	0.54
5763809 (F	30.01222	-98.2058	7/16/2015	24.54	82.2	13.8	7.01	1.19	0.36	0	288	27.3	12.3	0.2	2.61	7.47	300	Trinity	0.9379	-10.3	-21.7	-3.86	1.74
5763810	30.02861	-98.1775	6/1/2013	23.84	71.2	24.6	7.1	1.44	0.89	0	338	24.2	11.6	0.37	2.24	7.83	321	Trinity	0.6476	-10.6	-24	-3.98	1.09
5763813	30.01983	-98.1823	8/1/2023	23.64	218	147	315	19.5	6.41	0	223.3	1200	266	1.39	0.02	7.15	2297	Trinity					
5763814	30.03139	-98.1789	6/1/2023	22.53	88.2	20.3	9.82	1.09	0.429	0	355.1	24.9	15.9	0.33	5.755	7.11	351.8	Trinity	0.6242	-5.8	-22.88	-4.06	0.86
6805208	29.96083	-98.4275	6/1/1994	22	115	18	7.9	3.5	11.6	0	345.4	83	15	1.07	1.46	6.86	435	Trinity					
6805209	29.99139	-98.4281	8/1/2004	21.2	80.5	36.1	8.8	2.85	6.13	0	313.6	83.7	11.8	0.81	0.09	7.09	399	Trinity					
6805210	29.98611	-98.4297	6/1/2013	21.4	91.4	45.4	10	3.37	18.7	0	328.3	166	14.3	1.57	0.02	7.2	524	Trinity					
6805306	29.96383	-98.4055	7/1/2023	21.4	70.5	16.5	6.06	1.54	4.29	0	259.9	25.5	7.14	0.764	1.164	6.59	270.2	Trinity	0.2039	-0.7	-25.57	-4.52	0.52
6805312	29.99389	-98.3947	6/1/2015	21.2	112	21.8	7.38	49.1	15.9	0	301.4	20.9	168	0.61	1.79	6.81	558	Trinity					
6806302	29.96353	-98.2527	8/1/1995	0	93	19	9	0	0	0	350.2	17	15	0.4	3.2	7.9	328	Trinity					
6806303	29.96833	-98.255	8/1/1995	0	100	11	7	0	0	0	351.5	13	10	0.3	4.42	7.8	318	Trinity					
6806304	29.96806	-98.2525	8/1/1995	0	70	33	17	0	0	0	347.8	35	19	1	0.31	8	346	Trinity					
6806312	29.97611	-98.2644	7/1/2013	23.5	47.9	36.2	11.5	3.75	4.5	0	327.1	33.1	14.5	1.3	0.02	7.36	326	Trinity	0.0372	-5.6	-24.8	-4.14	-0.01
6806313	29.98137	-98.2614	8/1/2020	23.36	82.3	39.5	6.55	2.91	2.45	0	395.4	47.2	14.9	1.38	0.432	7.41	404.4	Trinity					
6807202	29.97745	-98.2055	5/1/2019	21.9	95.6	12.4	6.76	1.23	0.256	0	334.4	11.8	9.3	0.179	3.519	6.97	314.8	Trinity	0.7298	-11.3	-25.1	-4.23	1.45
6807408	29.95444	-98.2278	8/1/1995	0	58	36	21	0	0	0	338	38	19	1.3	0.84	8	340	Trinity					
6807409	29.95213	-98.2233	5/1/1997	0	54	34	24	0	0	0	324.6	44	28	1	0.4	7.6	345	Trinity					
5763809 (F	30.01222	-98.2058	10/5/2012	22.9	67.8	15.3	5.5	1.51	0.535	0	256.3	33.4	8.8	0.22	2.39	7.59	272	Trinity	0.9086	-11.7			1.92
5763809 (F	30.01222	-98.2058	11/19/2013	20.28	74.2	14.1	5.76	1.34	0.5	0	277	34.5	11.2	0.23	2.25	7.84	290	Trinity	0.9086	-14	-24.4	-3.96	1.65
5763809 (F	30.01222	-98.2058	9/14/2023	21.88	93.4	24.3	8.64	1.7	1.05	0	261	55.3	12	0.236		7.09	327	Trinity	0.7618	-9.1			
STUDE S	30.02722	-98.2603	9/12/2023	21.48	93.5	20.9	6.5	1.51	0.494	0	280	16.1	8.77	0.18		7.11	319	Trinity	0.7533	-9.6			
6806306	29.97657	-98.2625	9/28/2023	22.17	78.5	28.6	9.55	2.6	1.26	0	294	29	14	0.726	0.358	6.9	318	Trinity	0.503	-3.22	-22.9	-4.59	0.87
UBR2	-98.3417	30.09922	6/17/2008	31.6	39.28	25.28	12.41	2.346	0		200.7	27.86	20.92	0.152	0.248	7.9	365	Blanco River Water			6.52	3.57	
UBR6	-98.2003	30.00064	6/17/2008	28.8	86.97	20.42	7.587	1.173	0.8762		300.2	43.23	13.47	0.133	2.232	7.7	494	Blanco River Water			-25.81	-3.5	